Nanotechnology, Science and Applications

Dovepress
Taylor & Francis Group

Open Access Full Text Article

ORIGINAL RESEARCH

Safety Profile of Intravenous Ferulic Acid Nanoparticles: Acute Toxicity and Neurological Effects in Sprague-Dawley Rats

Hao Huang[1,2]*, Yan Xuan[3]*, Zeng-Chun Ma[4]

[1]GCP Institutional Office, The First People's Hospital of Neijiang, Neijiang, Sichuan, 641000, People's Republic of China; [2]Department of Clinical Pharmacy, Chengdu Qingbaijiang District People's Hospital, Chengdu, Sichuan, 610399, People's Republic of China; [3]Department of the 4th Division, Peking University School and Hospital of Stomatology & National Clinical Research Center for Oral Diseases. 22 Zhongguancun South Avenue, Haidian District, Beijing, 100081, People's Republic of China; [4]Beijing Institute of Radiation Medicine, Beijing, 100850, People's Republic of China

*These authors contributed equally to this work

Correspondence: Hao Huang; Zeng-Chun Ma, Email happyhh758@163.com; mazchun@139.com

Background: Ferulic acid (FA) exhibits therapeutic potential for various disorders, but its clinical application is hindered by poor bioavailability and solubility. This study aimed to develop and evaluate FA-loaded lipid nanoparticles (FA-LNPs) as a safe and efficient drug delivery system.

Methods: FA-LNPs were prepared via an optimized active loading method. The Morris water maze test was conducted to evaluate FA efficacy against LPS-induced cognitive impairment in rats. Comprehensive neurotoxicity assessment was performed in three brain regions (striatum, hippocampus, and cerebellum-brain stem) using multiple staining techniques (LFB, GFAP, IBA-1, and Fluoro-Jade) to evaluate myelin integrity, glial activation, and neuronal degeneration. Acute toxicity, pharmacokinetics, and network pharmacology analysis were conducted to assess safety profiles and potential mechanisms.

Results: FA-LNPs were successfully prepared using an optimized active loading method, achieving high drug loading (≥4 mg/mL), superior encapsulation efficiency (EE%) ≥80%, and uniform particle size distribution (<200 nm, PDI=0.053), zeta potential of +5.97 mV (Quality Factor = 1.701), excellent storage stability over two weeks, and was scaled up for batch production. The Morris water maze test revealed an effective FA concentration of 50 mg/kg, with FA-LNPs achieving 46.5 mg/kg through active loading method. Toxicological studies demonstrated favorable safety profiles. Pharmacokinetic analysis showed a prolonged elimination half-life (12.8 ± 1.88 hours) and moderate systemic clearance (0.535 ± 0.0851 L/h/kg). Short-term administration did not elicit significant neuroprotection. Network pharmacology analysis identified 141 potential therapeutic targets and five key proteins (EGFR, ESR1, PTGS2, CTNNB1, and STAT3), with molecular docking confirming favorable binding energies (−7.6 to −5.2 kcal/mol).

Conclusion: FA-LNPs enhanced FA's bioavailability without apparent systemic toxicity or neurotoxicity. While safe for short-term use, longer treatment durations may be necessary to observe potential neuroprotective benefits and toxicity. This study provides a foundation for further investigation of FA-LNPs as a promising drug delivery system for neurological disorders.

Keywords: ferulic acid, liposome nanoparticles, drug delivery, network pharmacology, pharmacokinetics, toxicology, Alzheimer's disease, atherosclerosis

Introduction

Ferulic acid [(E)-3-(4-hydroxy-3-methoxy-phenyl) prop-2-enoic acid; FA] belongs to the family of phenolic acids, is usually found in foods like rice, oats, wheat, vegetables, grasses, fruits, grains. FA and related ester derivatives decrease the levels of some inflammatory mediators, has high anti-inflammatory and antioxidant properties, being able to act as a scavenger of free radicals.[1–4] It has been postulated that administration of FA induces resistance to Aβ toxicity in mice and has been suggested to be useful as a chemo-preventive agent against AD.[5] Inflammation has been described as the culprit of disease or an attempt by the immune system to contain accumulation of Aβ plaques in the brain.[6] Some research works have revealed FA is capable of penetrating

Received: 24 October 2024
Accepted: 12 March 2025
Published: 28 July 2025

Graphical Abstract

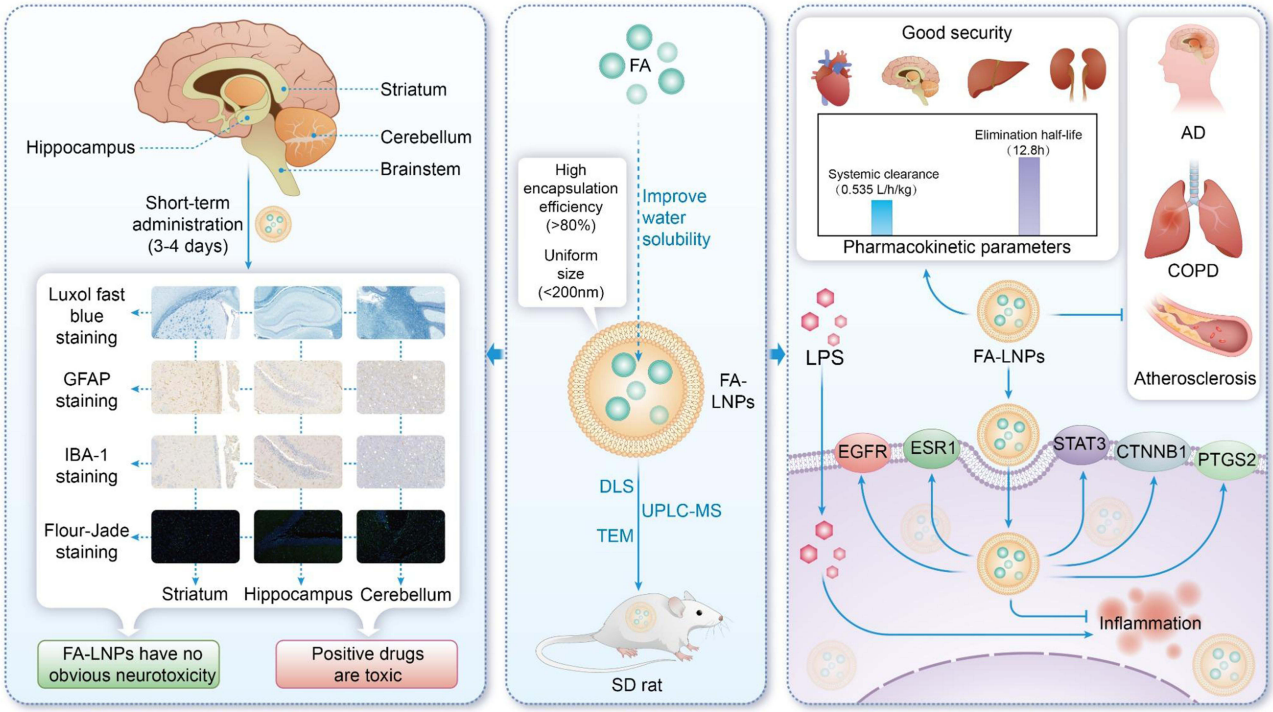

blood brain barrier (BBB), endowing it with opportunity to be available agents for brain diseases like AD.[7,8] Michels et al carry out study across species in larval Drosophila, adult flies and old (>2-year-old) mice, exploits the potential of the plant Rhodiola rosea and identifies the constituent FA eicosyl ester [icosyl-(2E)-3-(4-hydroxy-3-methoxyphenyl)-prop-2-enoate (FAE-20)] as a memory enhancer, these results may hold potential for clinical applications.[9] Chiaki Kudoh et al conducted a multicenter, randomized, double-blind, placebo-controlled prospective trial, and demonstrated the clinical effectiveness of FA and A. archangelica extract on cognitive functioning among older adult individuals with mild cognitive impairment (MCI).[10]

A number of antioxidant and/or anti-inflammatory including FA and related ester derivatives decrease the levels of some inflammatory mediators, such as TNF-α and IL-1β as well as their associated functions.[1–3]

Lipopolysaccharide (LPS) stimulates Toll-like receptors and induces strong expression of proinflammatory cytokines IL-1, IL-6 and TNF-α, primarily from macrophages.[11,12] Many physiological and behavioral deficit associated with LPS administration. LPS injection may affect performance in various learning tasks, Morris water maze (MWM) is included. Furthermore, LPS induced immune modulation of neural function may produce alterations in cognitive processes, including learning and memory.[13–15] Initially, we employed the Morris water maze test to evaluate the neuroprotective effects of FA against LPS-induced neurological damage in Sprague-Dawley (SD) rats following medium to long-term administration.

FA has garnered significant attention in neuroprotective research due to its potent antioxidant and anti-inflammatory properties.[16] However, the clinical application of FA faces substantial challenges due to its low water solubility and insufficient bioavailability.[17] To overcome these limitations, the development of novel drug delivery systems has become imperative.

Liposomal Nanoparticles (LNPs) have emerged as a promising drug delivery system, attracting considerable interest due to their ability to enhance drug solubility, improve bioavailability, and achieve sustained release effects.[18] Through optimization of preparation processes, we aim to address the poor solubility of FA post-administration, while simultaneously prolonging drug release time and improving the safety and stability of the formulation. This innovative delivery system holds the potential to significantly enhance the bioavailability of FA, thereby augmenting its therapeutic efficacy.[19]

The definition of nanomedicines varies among regulatory agencies, though all emphasize the significance of nanoscale dimensions and their associated unique properties. The European Medicines Agency (EMA) adopts a broader definition,

describing nanomedicines as products with at least one component in the 1–1000 nm range, emphasizing characteristics related to nanotechnology applications and anticipated clinical benefits,[20] In contrast, the US Food and Drug Administration (FDA) and the UK's Medicines and Healthcare products Regulatory Agency (MHRA) employ more stringent criteria, defining nanomedicine size ranges as 1–100 nm and 0.2–100 nm, respectively. These definitions appear to focus more on the unique physicochemical properties inherent to the nanoscale.[21] Notably, the FDA's definition includes an important supplementary clause: materials with dimensions up to the micron scale (1000 nm) may be considered nanomedicines if they exhibit unique physical, chemical, or biological properties associated with their nanoscale features. Liposomes, typically ranging from 100–400 nm, align with both EMA's definition and FDA's extended criteria.[22]

Nanomedicines can be broadly categorized into three main classes: carrier-based nanomedicines, drug nanoparticles, and other specialized types.[23] The nanoscale dimensions of these medicines, typically ranging from 1–1000 nm, confer unique physicochemical properties.[24] Due to their small size, nanomedicines possess exceptionally high surface-to-volume ratios, which enhance drug solubility and bioavailability.[25] Many nanosystems, particularly carrier-based nanomedicines, enable controlled drug release, prolonging therapeutic effects.[26] Certain nanomedicines demonstrate the ability to penetrate biological barriers, including cell membranes and nuclear envelopes.[27] These systems can achieve drug accumulation in specific tissues or cells through active or passive targeting mechanisms.[28]

These characteristics endow nanomedicines with tremendous potential for improving therapeutic efficacy, reducing side effects, and overcoming traditional drug delivery barriers. However, these same properties may present new challenges, such as potential long-term toxicity and immunogenicity concerns, which constitute the primary focus of many research investigation.

To comprehensively evaluate the biological effects of FA-LNPs, we conducted an extended acute toxicity study, encompassing general toxicity observations, hematological and biochemical parameter analyses, and histopathological examinations of major organs.

Neuroinflammation represents a hallmark pathological feature underlying various neurological disorders. FA has emerged as a promising therapeutic agent due to its potential neuroprotective properties.[17] While lipopolysaccharide (LPS)-induced neuroinflammation models have been extensively employed to investigate neuroinflammatory mechanisms and evaluate therapeutic interventions.[29] The therapeutic potential of FA-loaded liposomal nanoparticles in mitigating LPS-induced neuroinflammation and their comprehensive in vivo safety profiles warrant further investigation.

To elucidate the molecular mechanisms underlying FA-LNPs' therapeutic effects, we implemented an integrated approach combining network pharmacology and molecular docking analyses.[30] This systematic investigation revealed potential therapeutic targets and signaling pathways of FA across multiple pathological conditions, including Alzheimer's disease, Chronic Obstructive Pulmonary Disease (COPD), and atherosclerosis. Furthermore, this comprehensive study integrates advanced drug delivery systems, toxicological assessments, and mechanistic investigations to overcome the limitations associated with conventional FA administration. By harnessing liposomal nanotechnology and unraveling the molecular basis of FA's neuroprotective properties, our research provides a robust foundation for developing targeted therapeutic strategies for neurodegenerative disorders.

Materials and Methods

LPS Injections and Experimental Design

Animals and Experimental Design for Water Maze Test

Sixty Gender balanced Sprague-Dawley rats (250–300g, National Institutes for Food and Drug Control, China; License No: SCXK (Beijing): 2012–0001) were housed under standard laboratory conditions (25 ± 2°C, 50 ± 10% humidity, 12h light/dark cycle) with ad libitum access to food and water. All experimental procedures were approved by the Institutional Animal Care and Use Committee of Beijing Institute of Radiation Medicine and conducted in accordance with national guidelines.

Rats were randomly assigned to five groups (n = 12/group, 6 males and 6 females each): (1) Control (saline), (2) LPS (200 μg/kg), (3–5) LPS + FA (25, 50, or 100 mg/kg). FA was administered intraperitoneally (i.p.) daily for three weeks before LPS challenge. Subsequently, LPS (200 μg/kg, Sigma-Aldrich, USA) or vehicle was injected i.p. for five consecutive days. For behavioral studies, LPS was administered 4h prior to testing to ensure peak neuroinflammatory response (Figure 1).

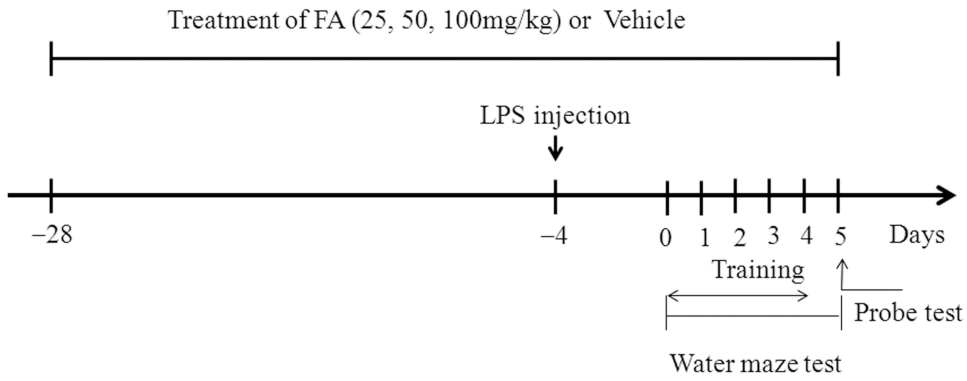

Figure 1 Experimental schedule of drug treatment and test orders. Arrow heads represent days on which acquisition tests were conducted. FA (25, 50, or 100mg/kg) or its vehicle (0.9% saline containing 10% DMSO) was i.p. injected for 24 consecutive days. Before the beginning of the four days visible platform test in the Morris water-maze, LPS (200 μg/kg) or its vehicle were i.p. injected 12 hours after FA or its vehicle injected. On day 29, the water-maze acquisition trials were conducted four times a day for four consecutive days, followed by the probe trial test 12 hours after the last acquisition trial.

Water Maze Test

The Morris water maze test was performed using SMG-2 system (Institute of Materia Medica, CAMS & PUMC) according to Morris et al [20], the apparatus consisted of a black circular pool (150 cm diameter × 50 cm height) filled with opaque water (22–25°C) to a depth of 30 cm. A transparent platform (11 cm diameter) was submerged 1.5 cm below water surface in the northeast quadrant. Fixed visual cues were displayed on surrounding walls. Animal movements were recorded by an overhead digital camera connected to a computer-based tracking system.

Synthesis of FA Liposomal Nanoparticles Using Microfluidic Devices

FA (purity ≥98%) was purchased from Sigma-Aldrich (USA). The Flow origin Lipo 1 lipid mixture kit (total lipid concentration 20 mg/mL) was provided by Mingtai Medical Equipment (Shanghai) Co., Ltd. Ultra-pure water (18.2 MΩ· cm, 25°C) was prepared using a Milli-Q system (Millipore, USA). All other reagents were of analytical grade.

FA Liposomal Nanoparticles (FA-LNPs) were prepared using a Microflow S microfluidic device (Nuohai Life Science co., Limited) via the aqueous/organic phase nanoprecipitation method. Briefly, FA was dissolved in the Flow origin Lipo 1 lipid mixture (organic phase, final concentration 10 mg/mL), with ultra-pure water serving as the aqueous phase. Both phases were loaded into separate syringes and connected to the microfluidic chip. Under optimized conditions, the aqueous and organic phases were mixed at a flow rate ratio of 3:1, with a total flow rate of 12 mL/min. The reaction was conducted at room temperature (25 ± 2°C). After discarding small amounts of initial and final waste liquid, the middle portion was collected as the final FA-LNPs product. Following each batch preparation, the product was filtered through a sterile 0.22 μm membrane to remove potential large particles.

The average particle size, polydispersity index (PDI), and Zeta potential of FA-LNPs were determined using dynamic light scattering (DLS). Freshly prepared FA-LNPs samples were diluted 20–30 times with 0.01 M NaCl solution or 10 mM Tris-HCl buffer (pH 7.4). Measurements were performed using a Zetasizer Pro nanoparticle analyzer (Malvern Panalytical, UK) at 25°C, with each sample measured in triplicate.

UPLC-MS Detection of Ferulic Acid

Chemicals and Reagents FA standard (analytical grade) was purchased from Sigma-Aldrich (catalog number 128708, St. Louis, MO, USA). Phosphate buffer (pH 7.4) containing approximately 1% ethanol, formic acid (analytical grade), ultrapure water, and acetonitrile (LC-MS grade) were obtained from Millipore Corporation (Billerica, MA, USA). HPLC-grade acetonitrile was sourced from Fisher Scientific (batch number 226049).

Instrumentation Chromatographic analysis was performed on an Acquity 2D-UPLC system coupled with an Acquity UPC2 system (Waters Corporation, Milford, MA, USA). Mass spectrometric detection was carried out using a Xevo G2-XS QTOF mass spectrometer equipped with an atmospheric pressure gas chromatography (APGC) source (Waters Corporation).

Sample Preparation A stock solution of FA (0.08 mg/mL) was prepared in phosphate buffer (pH 7.4) containing 1% ethanol. The solution was filtered through a 0.22 μm membrane filter prior to analysis.

Chromatographic Conditions Separation was achieved on an Acquity BEH C18 column (2.1 × 100 mm, 1.7 μm) maintained at 45°C. The mobile phase consisted of (A) water with 0.1% formic acid and (B) acetonitrile with 0.1% formic acid. The flow rate was set at 0.4 mL/min, and the injection volume was 1 μL. The gradient elution program was as follows: 0 min, 95% A; 3 min, 80% A; 10–12 min, 0% A; 15 min, 95% A.

Mass Spectrometry Conditions The mass spectrometer was operated in negative electrospray ionization (ESI) mode. Full scan data were acquired over the range of m/z 50–1000 with a scan time of 0.2 s. The optimized parameters were as follows: capillary voltage, 2.0 kV; sampling cone, 40 V; source temperature, 120°C; desolvation temperature, 450°C; cone gas flow, 60 L/h; desolvation gas flow, 800 L/h.

Data Analysis Data acquisition and processing were performed using MassLynx software (version 4.1, Waters Corporation). FA was identified by extracting the ion chromatogram at m/z 193.0506, corresponding to its deprotonated molecular ion [M-H]-. Collision energy was ramped from 10 to 45 eV for fragmentation studies.

Morphological Characterization of FA Liposomal Nanoparticles by Transmission Electron Microscopy

Sample preparation and transmission electron microscopy (TEM) observation were conducted according to the following protocol.

Hydrophilization of carbon support film: Standard carbon-coated copper grids were subjected to plasma treatment for 1 minute using a glow discharge system (PELco easiGlow™, TED PELLA, INC., USA) to enhance hydrophilicity.

Sample loading: The treated carbon-coated copper grids were secured with self-locking tweezers. A 4 μL aliquot of FA liposomal nanoparticle suspension was carefully deposited onto the carbon film surface using a precision pipette. After 1 minute, excess liquid was gently removed using filter paper (Whatman No.1).

Negative staining: Immediately following sample deposition, 4 μL of 2% phosphotungstic acid solution (2% w/v, pH 6.5, GZ02536-5, RXSY-CHEM, China) was applied to the sample. After 30 seconds, excess stain was carefully removed using filter paper.

Sample drying and TEM observation: The prepared samples were air-dried at room temperature for approximately 10–15 minutes. Observations were conducted using a Talos L120C G2 transmission electron microscope (Thermo Fisher, USA) at an accelerating voltage of 120 kV.

Image acquisition and analysis: High-resolution digital images were captured using the integrated CCD camera. Quantitative analysis of particle size and morphology was performed using ImageJ software (NIH, USA).

Precautions: All steps were performed in a clean environment to avoid sample contamination. The negative staining process was carefully timed to achieve optimal contrast. During observation, electron beam exposure was minimized to reduce sample damage.

Optimized Preparation and Characterization of FA Liposomal Nanoparticles (FA-LNPs)

Materials

FA (purity ≥98%) was purchased from Sigma-Aldrich (USA). Egg phosphatidylcholine (LIPOID E80) was supplied by LIPOID GmbH (Germany). Cholesterol was obtained from Avanti Polar Lipids (China). Sucrose (analytical grade) was purchased from Merck KGaA (Germany). Other reagents of analytical grade were procured from Sinopharm Chemical Reagent Co., Ltd (China). Ultra-pure water was prepared using a Milli-Q system (Millipore, USA).

Establishment and Validation of Analytical Methods

UV Spectrophotometry

A UV-1100 spectrophotometer (MAPADA, China) was used for FA content determination. The scanning wavelength range was 200–400 nm, with the maximum absorption wavelength identified at 310 nm. A series of FA ethanol solutions

(1.25–20 μg/mL) were prepared as standard curves. The absorbance of blank liposomes at 310 nm was 0.003, showing no significant interference with FA content determination.

Content Determination Method

FA reference standards were accurately weighed and prepared in ethanol to create a series of standard solutions (20, 10, 5, 2.5, 1.25 μg/mL). For sample analysis, 10 μL of the preparation was diluted 1000-fold with ethanol. Absorbance was measured at 310 nm, and FA content was calculated using the standard curve. Y=0.0777x+0.0024 (R^2=0.9999)

Encapsulation Efficiency Determination

Ultrafiltration centrifugation was employed to separate free drug. 200 μL of the preparation was placed in a 100 kDa ultrafiltration centrifuge tube (Millipore, UFC8100, USA) and centrifuged at 9000 g for 5 min (Eppendorf 5804R, Germany). 10 μL of the filtrate was diluted 1000-fold with ethanol for free drug analysis. Total content sample solution was prepared as described in Content Determination Method. FA concentrations in both total (C total) and free (C free) sample solutions were determined. Encapsulation efficiency (%) was calculated using the following formula:

$$\text{Encapsulation Efficiency (EE\%)} = (C_{total} - C_{free}) / C_{total} \times 100\%$$

Particle Size and Polydispersity Index Determination

A Zetasizer Pro nanoparticle analyzer (Malvern Panalytical, UK) was used to measure the average particle size and polydispersity index (PDI) of liposomes. 20 μL of the preparation was diluted 50-fold with ultra-pure water for measurement, with each sample measured in triplicate.

Preparation of FA Liposomal Nanoparticles

Lipid Film Hydration Method

Ferulic acid, egg phosphatidylcholine, and cholesterol were dissolved in chloroform: methanol (2:1, v/v) at a mass ratio of 1:10:2. Organic solvents were evaporated using a rotary evaporator (BUCHI, R-300, Switzerland) at 40°C under reduced pressure to form a uniform thin film. The film was hydrated with PBS (pH 7.4) containing 5% (w/v) sucrose for 30 min. The mixture was then sonicated intermittently for 5 min using a probe sonicator (Sonics, VCX 130, USA) at 40% power (10 s on, 5 s off). The resulting suspension was extruded 21 times through a liposome extruder (AVESTIN, LiposoFast-Basic, Canada) using membranes with pore sizes of 400 nm, 200 nm, and 100 nm (7 times each). Finally, the preparation was filtered through a 0.22 μm sterile membrane to obtain batch 230826–1.

Aqueous Preparation Method

FA was dissolved in 0.1 M NaOH solution and adjusted to pH 7.4. Egg phosphatidylcholine and cholesterol were dissolved in ethanol at a mass ratio of 10:2. The organic phase was slowly injected into the aqueous phase (1:9, v/v) under stirring (600 rpm). The mixture was sonicated and extruded as described in Lipid Film Hydration Method. Unencapsulated FA was removed by dialysis (MWCO 3500 Da) for 24 h. The final preparation was filtered through a 0.22 μm membrane to obtain batch 230826–3.

Active Loading Method

Blank liposomes were first prepared by dissolving egg phosphatidylcholine and cholesterol in ethanol (mass ratio 10:2) and slowly injecting into an aqueous solution containing 0.3 M $(NH_4)_2SO_4$ (1:9, v/v). After sonication and extrusion, external $(NH4)_2SO_4$ was removed by 24 h dialysis. Separately, FA was dissolved in 0.1 M NaOH and adjusted to pH 7.4. The FA solution was mixed with blank liposomes at a 1:2 (v/v) ratio and incubated at 37°C for 30 min. The final product was obtained by filtering through a 0.22 μm membrane. The preparation process was optimized by adjusting parameters such as pH (6.5–8.0), type of alkali (NaOH, Na_2CO_3), and incubation time (15–60 min).

Process Scale-Up and Batch Production

Based on the optimized active loading method, the preparation scale was increased to accommodate a total FA amount of ≥1 g. Particle size, PDI, content, and encapsulation efficiency were determined using the methods described in Establishment and Validation of Analytical Methods. Corresponding blank liposomes were prepared as a control, with a total volume of 40 mL.

Acute Toxicity Study of Intravenous FA Nanoparticles in SD Rats

Materials

Test and Control Articles FA nanoparticles (Batch No: 231220–1, 4.65 mg/mL) were obtained from Beijing Dona Pharmaceutical Technology Co., Ltd. 0.9% Sodium chloride injection (Batch No: SC23090303) was purchased from Shandong Hualu Pharmaceutical Co., Ltd. Lipopolysaccharide (LPS, Batch No: 0000228772) was sourced from Sigma-Aldrich, USA. Blank liposomes (Batch No: 231220–2) were provided by Beijing Dona Pharmaceutical Technology Co., Ltd.

Experimental Animals Specific-pathogen-free (SPF) SD rats (42–55 days old, 175–202 g, equal numbers of males and females) were obtained from Beijing Vital River Laboratory Animal Technology Co., Ltd. (License No: SCXK (Beijing) 2021–0006). Housing conditions complied with GB 14925–2010 standards. The study protocol was approved by the Institutional Animal Care and Use Committee (IACUC).

Experimental Design and Administration

Forty-two Sprague-Dawley rats (21 males and 21 females, weighing 200 ± 20 g) were randomly allocated into seven experimental groups (n=6/group, 3 males and 3 females per group). The groups comprised: blank control receiving 0.9% sodium chloride injection, vehicle control administered with blank liposomes (Con-LNPs), positive control treated with LPS (200 μg/kg), FA-LNPs group receiving FA nanoparticles (46.5 mg/kg × 2), LPS group administered with LPS (200 μg/kg), combination group treated with both LPS (200 μg/kg) and FA-LNPs (46.5 mg/kg/day), and a pharmacokinetic group receiving FA-LNPs (46.5 mg/kg).

All administrations were performed via tail vein injection at a volume of 10 mL/kg body weight. For acute toxicity evaluation (Groups 1–4), animals received two doses of respective treatments within 24 hours and were monitored for 7 consecutive days. For neuroprotective assessment (Groups 5–6), Group 5 received a single dose of LPS (200 μg/kg), while Group 6 received an initial LPS dose followed by daily FA-LNPs administration for 4 consecutive days. The first day of administration was designated Forty-two Sprague-Dawley rats (21 males and 21 females, weighing 200 ± 20 g) were randomly allocated into seven experimental groups (n=6/group, 3 males and 3 females per group). The groups comprised: blank control receiving 0.9% sodium chloride injection, vehicle control administered with blank liposomes (Con-LNPs), positive control treated with LPS (200 μg/kg), FA-LNPs group receiving FA nanoparticles (46.5 mg/kg × 2), LPS group administered with LPS (200 μg/kg), combination group treated with both LPS (200 μg/kg) and FA-LNPs (46.5 mg/kg/day), and a pharmacokinetic group receiving FA-LNPs (46.5 mg/kg) on Day 1 (D1). Group 7 received a single dose of FA-LNPs (46.5 mg/kg) for pharmacokinetic analysis. Detailed experimental design and grouping information are provided in Table 1.

Observation Parameters and Detection Methods

General Condition

Observation All animals were observed twice daily for toxicity reactions, symptom severity, onset time, duration, and recovery time. Groups I–IV underwent more frequent observations post-dosing on Day 1 (D1).

Body Weight Measurement

Body weights were measured using an electronic balance (BSA2201-CW, Sartorius) at consistent times. All animals were weighed twice before dosing. Groups I–IV were weighed daily during the dosing period, while Groups V–VII were weighed on dosing and necropsy days.

Food and Water Consumption

Daily food and water intake were measured for Groups I–IV from D1 onwards. Average daily consumption per animal was calculated.

Table 1 Experimental Design and Group Allocation for Evaluating the Acute Toxicity, Neuroprotective Effects and Pharmacokinetics of FA-LNPs in Rats

Group	Subgroup	Treatment	Dose	Concentration (mg/mL)	Experimental Day	Animal ID
I	Blank control	0.9% NaCl	–	–	D1:Administration D7: End of observation	M: 1–3 F: 4–6
II	Vehicle control	Con-LNPs	–	–	D1: Administration D7: End of observation	M: 7–9 F: 10–12
III-1	Positive control	LPS	200 μg/kg	–	D1: Administration D7: End of observation	M: 13–15 F: 16–18
III-2	Positive control	LPS	100 μg/kg	–	D1: Administration D7: End of observation	M: 43–45 F: 46–48
IV	FA-LNPs	FA-LNPs	93 mg/kg	4.65	D1: Administration D7: End of observation	M: 19–21 F: 22-24
V	LPS	LPS	200 μg/kg	–	D1: First administration D4: Tissue collection	M: 49–51 F: 52-54
VI	LPS + FA-LNPs	LPS + FA-LNPs	LPS: 200 μg/kgFA-LNPs: 46.5 mg/kg	4.65	D1: First administration D4: Last administration and tissue collection	M: 55–57 F: 58-60
VII	Pharmacokinetics	FA-LNPs	46.5 mg/kg	4.65	D4: Administration D6: Last blood collection	M: 37–39 F: 40–42

Notes: The experimental groups were as follows: Control Group: Animals were administered 0.9% sodium chloride injection. Positive Control Group (LPS Group): Animals were administered lipopolysaccharide (LPS). Test Compound Group (FA-LNPs Group): Animals were administered ferulic acid encapsulated in liposomal nanoparticles. LPS + Test Compound Group (LPS+FA-LNPs Group): Animals were administered LPS followed by ferulic acid liposomal nanoparticles. This grouping design allows for the evaluation of the effects of LPS-induced inflammation and the potential protective effects of ferulic acid liposomal nanoparticles in a controlled experimental setting.
Abbreviations: M, Male; F, Female; LPS, Lipopolysaccharide; NaCl, Sodium chloride.

Hematology and Clinical Chemistry

Blood samples were collected at the end of the observation period following a 12–16 hour fast (water allowed). Sampling details for hematology and clinical chemistry analyses (Table 2). Analyses were performed using automated hematology and biochemistry analyzers (Table 3). Serum biochemistry parameters, measurement methods, and instrumentation (Table 4). Animal sample information for various indicators tested at different stages of the experiment (Table 5).

Organ Weights and Coefficients

Heart, liver, kidney, and brain weights were measured at the end of the observation period. Organ coefficients were calculated as (organ weight / body weight) × 100%.

Blood Drug Concentration

For Group VII, blood samples were collected pre-dose and at 1 min, 10 min, 30 min, 1 h, 3 h, 6 h, 24 h, and 48 h post-dose. Processed samples were stored at −70°C until analysis.

Table 2 Blood Sampling Protocols for Hematological and Clinical Chemistry Analyses

Parameter	Sampling Method	Sample Volume	Sampling Time	Notes
Hematology	Abdominal aorta blood collection	1 mL	End of observation period (Day 7)	EDTA-K2 anticoagulant
Clinical chemistry	Abdominal aorta blood collection	3 mL	End of observation period (Day 7)	Procoagulant

Table 3 Complete Blood Count Parameters and Their Analytical Methods

Parameter	Abbreviation	Method	Instrument
Red blood cell count	RBC	2D flow cytometry	ADVIA 2120i Automated Hematology Analyzer
Hemoglobin	HGB	Colorimetry	
Hematocrit	HCT	Calculation	
Mean corpuscular volume	MCV	2D flow cytometry	
Mean corpuscular hemoglobin	MCH	Calculation	
Mean corpuscular hemoglobin concentration	MCHC	Calculation	
White blood cell count	WBC	Flow cytometry	
Neutrophil count	NEUT	Flow cytometry	
Lymphocyte count	LYM	Flow cytometry	
Monocyte count	MONO	Flow cytometry	
Eosinophil count	EOS	Flow cytometry	
Basophil count	BASO	Flow cytometry	
Neutrophil percentage	NEUT%	Calculation	
Lymphocyte percentage	LYM%	Calculation	
Monocyte percentage	MONO%	Calculation	
Eosinophil percentage	EOS%	Calculation	
Basophil percentage	BASO%	Calculation	
Platelet count	PLT	2D flow cytometry	
Mean platelet volume	MPV	2D flow cytometry	
Reticulocyte count	Reti	Flow cytometry	
Reticulocyte percentage	Reti%	Calculation	

Table 4 Biochemical Parameters and Analytical Methods Using Automated Chemistry Analyzer

Parameter	Abbreviation	Method	Instrument
Alanine aminotransferase	ALT	IFCC kinetic method	BECKMAN COULTER AU480 Automated Biochemistry Analyzer
Aspartate aminotransferase	AST	IFCC kinetic method	
Alkaline phosphatase	ALP	IFCC kinetic method	
Total protein	TP	Biuret endpoint method	
Albumin	ALB	Bromocresol green endpoint method	
Total bilirubin	TBIL	Vanadate oxidation method	
Creatinine	CREA	Jaffe kinetic method	
Urea	UREA	Urease-GLDH method	
Uric acid	UA	Uricase-POD method	

(*Continued*)

Table 4 (Continued).

Parameter	Abbreviation	Method	Instrument
Creatine kinase	CK	IFCC kinetic method	
Triglycerides	TG	GPO-PAP method	
Total cholesterol	CHOL	CHOD-PAP method	
Lactate dehydrogenase	LDH	LD-L kinetic method	
Glucose	GLU	Glucose oxidase method	
Calcium	Ca	o-Cresolphthalein complexone method	
Globulin	GLB	Calculated	
Albumin/Globulin ratio	A/G	Calculated	
Sodium	Na	Ion-selective electrode	
Potassium	K	Ion-selective electrode	
Chloride	Cl	Ion-selective electrode	

Table 5 Schedule of Laboratory Evaluations and Necropsy Time Points for Toxicological Assessment

Parameter	Study Stage	Animal ID	Number of Animals
Hematology and Clinical Chemistry	D7	Group I: ♂1-3, ♀4-6	23
		Group II: ♂7-9, ♀10-12	
		Group III: ♂13-15, ♀17-18	
		Group IV: ♂19-21, ♀22-24	
Necropsy	D2	Group III: ♀16	1
	D2	Group V: ♂51	1
	D4	Group V: ♂49-51, ♀52-54	11
		Group VI: ♂55-57, ♀58-60	
	D7	Group I: ♂1-3, ♀4-6	23
		Group II: ♂7-9, ♀10-12	
		Group III: ♂13-15, ♀17-18	
		Group IV: ♂19-21, ♀22-24	

Data Collection and Result Interpretation

Data collection was performed using the Provantis 10.5.0.4 system or a higher version. Various parameters were recorded in different modules of the system. The in vivo experimental module was used to collect data on quarantine records, cage-side observations, drug administration, body weight, and food consumption. Clinical pathology parameters, including hematology and serum biochemistry indices, were automatically transmitted to the clinical pathology module following instrument analysis. Pathological data, such as gross observations and organ weights, were recorded in the pathology module.

Water consumption was initially recorded on paper forms and subsequently entered into the system. Other data were also documented using paper forms. In the Provantis system, this study corresponds to the source study S-TS23085-DJ and the target study T-TS23085-DJ.

This systematic approach to data collection and management ensures accuracy, traceability, and efficient analysis of the experimental results.

Histopathological Examination

Hematoxylin-Eosin (H&E) Staining

Pathology case numbers and organ inventory required (Table 6). Sections were deparaffinized, rehydrated, and stained following standard H&E protocol. Briefly, sections were stained with hematoxylin (4 min), differentiated in 1% acid alcohol, and counterstained with 0.5% Eosin Y (1 min). A total of 180 slides were prepared, with 39 representative slides digitally scanned using a Pannoramic 250 Flash III Scanner (3DHISTECH, Hungary).

Immunohistochemistry

Sections underwent antigen retrieval (EDTA solution, 140°C, 3 min) and blocking procedures. Primary antibodies against GFAP (1:3000, Sigma-Aldrich) and Iba1 (1:3000, Sigma-Aldrich) were applied overnight at 4°C, followed by HRP-conjugated secondary antibodies. Immunoreactivity was visualized using DAB substrate.

Special Staining Procedures

Fluoro-Jade B (FJB) Staining

For neuronal degeneration assessment, sections were incubated in FJB working solution (Biosensis) overnight at 4°C, counterstained with DAPI, and evaluated using a standardized scoring system.

Luxol Fast Blue (LFB) and Cresyl Violet Staining

Sections were stained with Solvent Blue 38 solution (60°C, 2h), differentiated in lithium carbonate solution, and counterstained with Cresyl Violet acetate.

Table 6 Pathology Case Numbers and Organ Inventory Required

Group	Subgroup	Treatment	Dose	Animal ID		Number of Animals	Organs Collected
				Male	Female		
I	Acute toxicity	Blank control	–	1-3	4-6	6	Heart, Liver, Kidney, Brain
II	Acute toxicity	Vehicle control	-	7-9	10-12	6	Heart, Liver, Kidney, Brain
III-1	Acute toxicity	High-dose positive control	LPS: 200 μg/kg	13-15	16-18	6	Heart, Liver, Kidney, Brain
III-2	Acute toxicity	Low-dose positive control	LPS: 100 μg/kg	43-45	46-48	6	Heart, Liver, Kidney, Brain
IV	Acute toxicity	FA-LNPs	93 mg/kg	19-21	22-24	6	Heart, Liver, Kidney, Brain
V	Pharmacological pathology	LPS	200 μg/kg	49-51	52-54	6	Brain
VI	Pharmacological pathology	LPS + FA-LNPs	LPS: 200 μg/kg FA-LNPs: 46.5 mg/kg	55-57	58-60	6	Brain

Image Analysis and Quantification

Immunoreactivity was visualized using DAB substrate and counterstained with hematoxylin. All sections were digitized using a Pannoramic 250 scanner (3DHISTECH, Hungary). Three specific brain regions were examined: striatum, hippocampus, and cerebellar-brainstem areas, as defined by "The Mouse Brain in Stereotaxic Coordinates - 4th Edition" (Figure 2). Quantitative assessments included GFAP-positive area percentage, Iba-1-positive area ratio and cell rate, gray/white matter distribution in LFB staining. FJB staining was evaluated using a semi-quantitative scoring system. The scoring criteria were as supporting information Table 7. Two independent pathologists, blinded to treatment groups, evaluated all histological samples.

Network Pharmacology Analysis

The potential mechanism of FA was investigated through network pharmacology approach. Briefly, FA-related targets were predicted using SwissTargetPrediction and Super-PRED databases (n=176). Disease-associated targets were collected from GeneCards, OMIM, CTD, and DisGenet databases using keywords "Alzheimer's Disease", "COPD", "AECOPD", and "Atherosclerosis" (n=47,043). The intersection analysis identified 141 common targets.

The compound-target-disease network was constructed using Cytoscape 3.9.0. The protein-protein interaction (PPI) network was generated via STRING database (minimum interaction score=0.400) and the top 5 hub targets were identified based on degree values. GO and KEGG pathway enrichment analyses were performed using DAVID platform ($P<0.05$, $Q<0.05$).

For molecular docking, the 3D structures of FA and key target proteins were obtained from PubChem and RCSB PDB databases, respectively. AutoDock was employed for docking simulation after proper protein preparation. The binding modes were analyzed using Discovery Studio.

Statistical Methods

Statistical Analysis for Expanded Acute Toxicity Study of Intravenous FA Nanoparticles in SD Rats

All statistical analyses were performed using two-tailed tests with a significance level set at 0.05. Mean, standard deviation SD, and sample size N for all group results were calculated using the Provantis system SAS 9.4 statistical software for parameters including body weight, organ weight, clinical pathology indices, and other relevant indicators. Data analysis followed this procedure:

First, Shapiro–Wilks test and Levene's test were used to assess normality and homogeneity of variance. If both tests were non-significant $P > 0.05$, one-way ANOVA was performed. For significant ANOVA results $P \leq 0.05$, Dunnett's test was used for multiple comparisons.

If normality and/or homogeneity of variance tests failed $P \leq 0.05$, data were log-transformed and retested. If post-transformation tests were non-significant $P > 0.05$, one-way ANOVA was conducted. For significant results $P \leq 0.05$, data underwent rank transformation.

After rank transformation, Kruskal–Wallis test was applied. For significant Kruskal–Wallis test results $P \leq 0.05$, Wilcoxon test was used for multiple comparisons.

Log transformation was not performed on data containing negative values. For data with zero values, these were replaced with one-tenth of the smallest positive value before log transformation. Statistical comparisons were not performed for sample sizes less than 3.

Cage-side observations were not statistically analyzed but presented as individual data and/or frequency counts.

Other Statistical Analyses

Data are presented as mean ± standard error of the mean (SEM). Statistical analyses were performed using GraphPad Prism software (version 8.0, GraphPad Software Inc., San Diego, CA, USA). Comparisons between groups were made using one-way analysis of variance (ANOVA) followed by Tukey's post hoc test or two-way ANOVA followed by Sidak's multiple comparisons test. $P < 0.05$ was considered statistically significant.

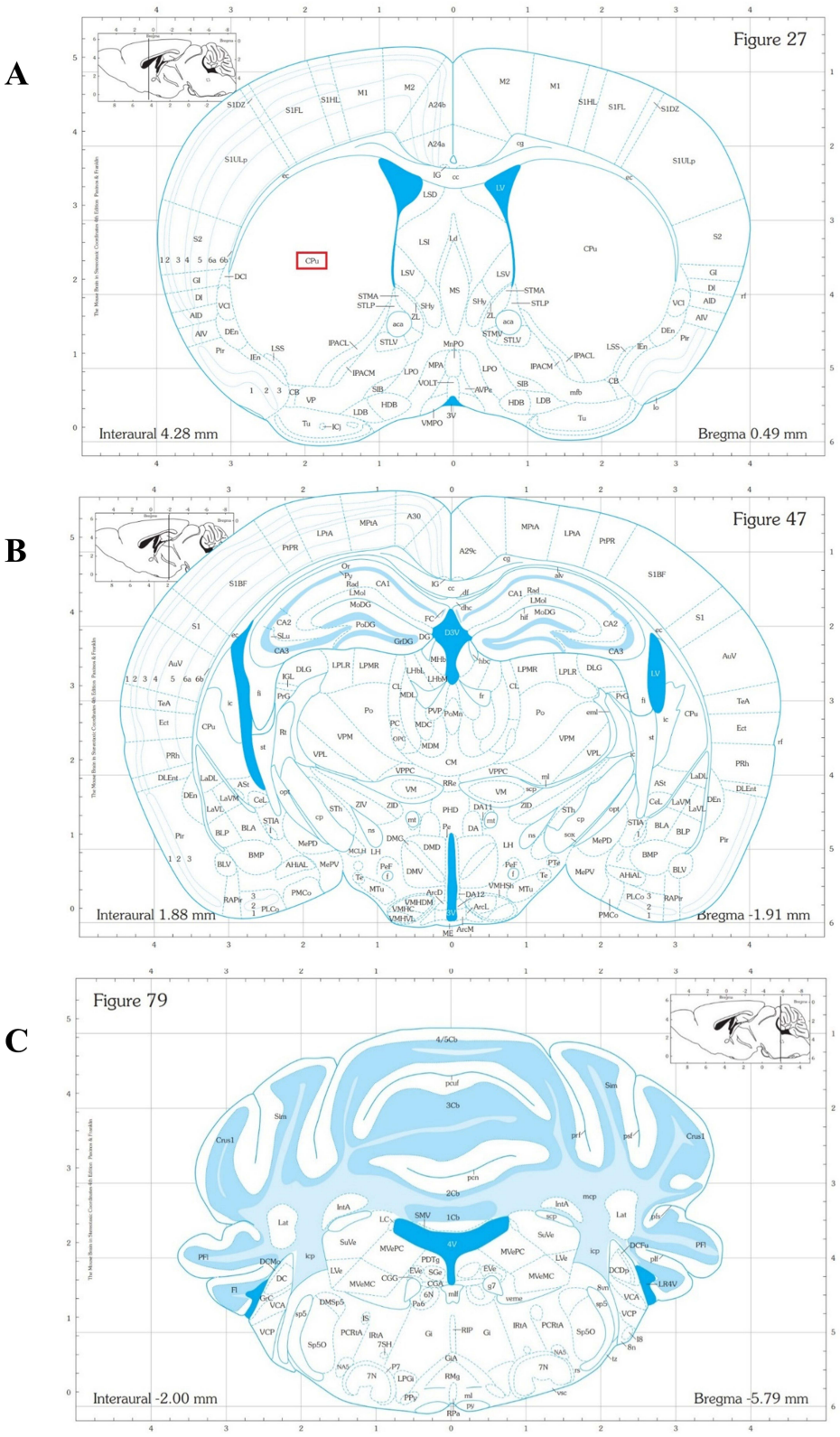

Figure 2 The core brain regions for observation. The core brain regions of interest for observation encompassed the striatum, hippocampus, and cerebellar-brainstem areas, we referenced Figures 27, 47, and 79 from "The Mouse Brain in Stereotaxic Coordinates - 4th Edition" (Paxinos and Franklin, 2012) as illustrated in Figure 2 (**A**–**C**).

https://doi.org/10.2147/NSA.S500407

Table 7 Scoring Criteria for Fluoro-Jade B Staining in Neuronal Degeneration Assessment

Score	Criteria
0	No neuropathology
1	Minimal/very few neuropathological changes (1–10% of neurons stained)
2	Mild neuropathology (11–25% of neurons stained)
3	Moderate neuropathology (26–45% of neurons stained)
4	Severe neuropathology (>45% of neurons stained)

Results

Effects of FA on LPS Induced Memory Impairments

Spatial learning and memory were assessed using the Morris water maze test. During the four-day training phase (4 trials/day), all groups showed progressive improvement in escape latency (Figure 3A and B). LPS-treated rats exhibited significantly longer escape latency but shorter swimming distance compared to controls, indicating LPS-induced bradykinesia (Figure 3C and D).

In the probe trial (24h after the last training session), LPS administration significantly impaired spatial memory, as evidenced by decreased time spent in the target quadrant, reduced swimming distance, slower swimming speed, and fewer platform area crossings. FA pretreatment effectively prevented these LPS-induced cognitive deficits (Figure 3E–H).

Characterization of FA-LNPs

UPLC-MS Analysis and TEM Observation

The molecular composition of FA-LNPs was characterized using UPLC-MS analysis. A characteristic peak at *m/z* 193.0501 with a retention time of 3.09 min confirmed the presence of ferulic acid (FA) in the nanoparticles (Figure 4 and Table 8). Transmission electron microscopy (TEM) imaging revealed an average particle size of approximately 80 nm (Figure 5), consistent with dynamic light scattering (DLS) measurements (Z-Average diameter: 83.85 nm, PDI = 0.053) (Figure 6). These results demonstrate the successful synthesis of FA-LNPs with uniform size distribution and well-defined morphology.

Zeta Potential and Stability

The zeta potential measurements were performed using a Zetasizer (DTS1070 cell) at 25°C. The nanoparticles were dispersed in water (dispersant RI = 1.33, viscosity = 0.88 cP, dielectric constant = 78.5). The samples were prepared using polystyrene latex (RI = 1.59, absorption = 0.01) as the material.

The zeta potential was measured at +5.969 mV with a conductivity of 0.0128 mS/cm, suggesting moderate stability of the nanoparticle system. The wall zeta potential was 14.31 mV, with a zeta deviation of 5.444 mV. The quality factor of 1.701 further confirmed the reliability of the measurements. Despite the relatively low zeta potential value, the nanoparticle formulation demonstrated excellent stability over two weeks, with no significant changes in size or polydispersity, which could be attributed to the optimized preparation process and the unique surface properties of the nanoparticles (Figure 7).

Scale-Up and Optimization of FA-LNP Preparation

Microfluidic Technology

FA-LNPs prepared via microfluidic technology demonstrated exceptional uniformity, with a Z-Average diameter of 83.85 nm and a remarkably low PDI of 0.053. This approach enables rapid evaluation of formulation feasibility through precise control of particle formation parameters.[31] However, the drug concentration achieved by this method was insufficient for in vivo administration, highlighting its utility as a screening tool rather than a production method.

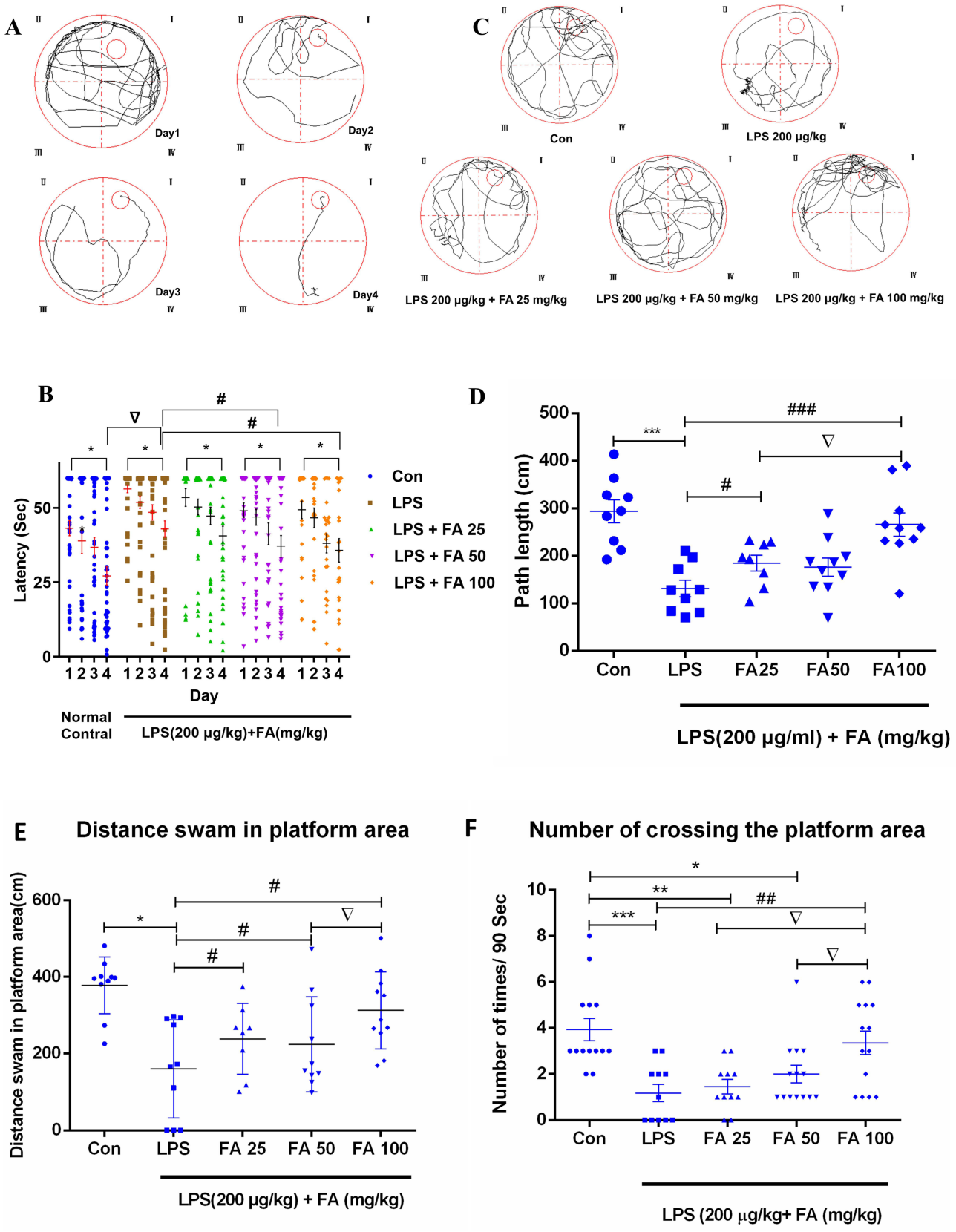

Figure 3 Continued.

https://doi.org/10.2147/NSA.S500407

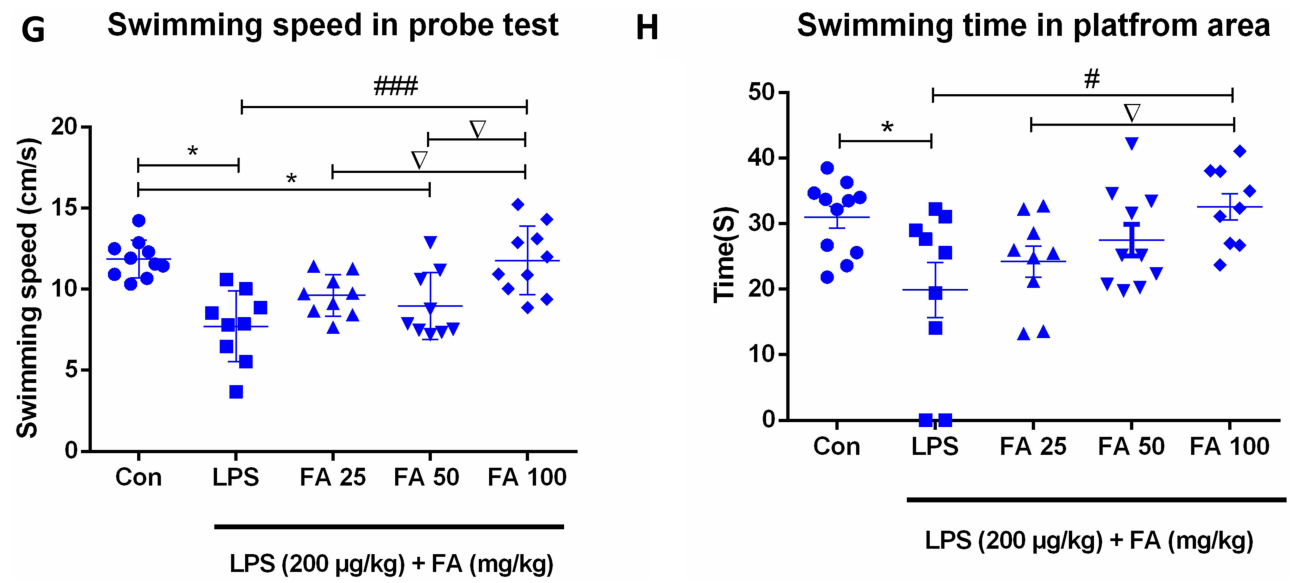

Figure 3 Effects of FA on LPS-induced spatial cognitive deficits in the water-maze test in rats. (**A**) Representative searching swimming paths by rats with different treatments after four days acquisition session in the escape latency test. (**B**) Escape latency to find the submerged platform during 4 consecutive days of training. LPS administration (200 μg/kg) significantly impaired spatial learning, demonstrated by increased escape latency compared to control group. Pretreatment with ferulic acid (FA) at 25, 50, and 100 mg/kg dose-dependently attenuated this LPS-induced learning deficit. All groups showed effective learning as indicated by significantly reduced escape latency between Day 1 and Day 4. Data are presented as individual data points with means ± SEM (n=12/group). Statistical analysis was performed using two-way ANOVA followed by Sidak's multiple comparisons test. * $p<0.05$ indicates significant differences between Day 1 and Day 4 within the same group, demonstrating effective training; $^{\triangledown}$ $p<0.05$ indicates significant difference between control and LPS groups on Day 4, demonstrating LPS-induced cognitive impairment; $^{\#}$ $p<0.05$ indicates significant differences between LPS group and FA treatment groups, demonstrating the protective effects of FA against LPS-induced cognitive dysfunction. (**C**) Representative searching swimming paths by rats with different treatments in the probe trial test. Control group rats swam concentrating the hidden platform area, LPS-treated rats swam primarily around the pool; this was reversed by FA pretreatment. (**D**) Effects of FA on the escape latency to reach the hidden platform. LPS overall decreased escape latency, which is altered by FA. E to H. Effects of FA pretreatment in the probe trial test with or without LPS stimulation in rats. (**E**) Distance swum in the target quadrant, (**F**) Number of crossing the hidden platform area, (**G**) Mean swimming speed in the probe trial test, (**H**) Duration in the hidden platform area. LPS decreased the swimming distance, the crossings, swimming speed and duration in the target quadrant, which were all reversed by FA (25, 50, or 100 mg/kg), whereas not in a strict dose-dependent manner. Values represent means ± S.E.M. (n=12 per group); * $p<0.05$, ** $p<0.01$, *** $p<0.001$ vs control group; $^{\#}$ $p<0.05$, $^{\#\#}$ $p<0.01$, $^{\#\#\#}$ $p<0.001$ vs LPS group; $^{\triangledown}$ $p<0.05$ for comparisons between different FA dosage groups (specifically indicating significant differences between FA 25 mg/kg vs FA 50 mg/kg or FA 100 mg/kg groups).

Lipid Solubilization Method

Initial attempts using the lipid solubilization method resulted in large, non-uniform particles (batch 230826–1) with low encapsulation efficiency (3.10 mg/mL vs theoretical 5 mg/mL). Rapid turbidity formation and FA precipitation upon hydration rendered this method unsuitable for FA-LNP development (Table 9).

Aqueous Preparation Method

The aqueous method also proved ineffective, as a significant portion of FA remained unencapsulated. Post-dialysis FA concentrations were excessively low, failing to meet preparation criteria (Table 10).

Active Loading Method

The active loading method enabled efficient FA encapsulation, achieving a concentration ≥4 mg/mL and encapsulation efficiency ≥80%. The optimized process yielded uniform particles (size ≤200 nm, PDI ≤0.2) suitable for animal administration (Tables 11–13). FA-LNPs exhibited a zeta potential of +5.97 mV, indicating moderate colloidal stability. The quality factor of 1.701 further confirmed the reliability of the measurements. The nanoparticles showed excellent storage stability over two weeks, with no significant changes in size or polydispersity.

Significance of Preparation Methods and Nano-Toxicity Considerations

The comparison of preparation methods highlights the superiority of the active loading approach in achieving high encapsulation efficiency and uniform particle size. The zeta potential results (+5.97 mV) further support the stability and suitability of FA-LNPs for in vivo applications. The sub-100 nm size of our FA-LNPs, potential nanotoxicity

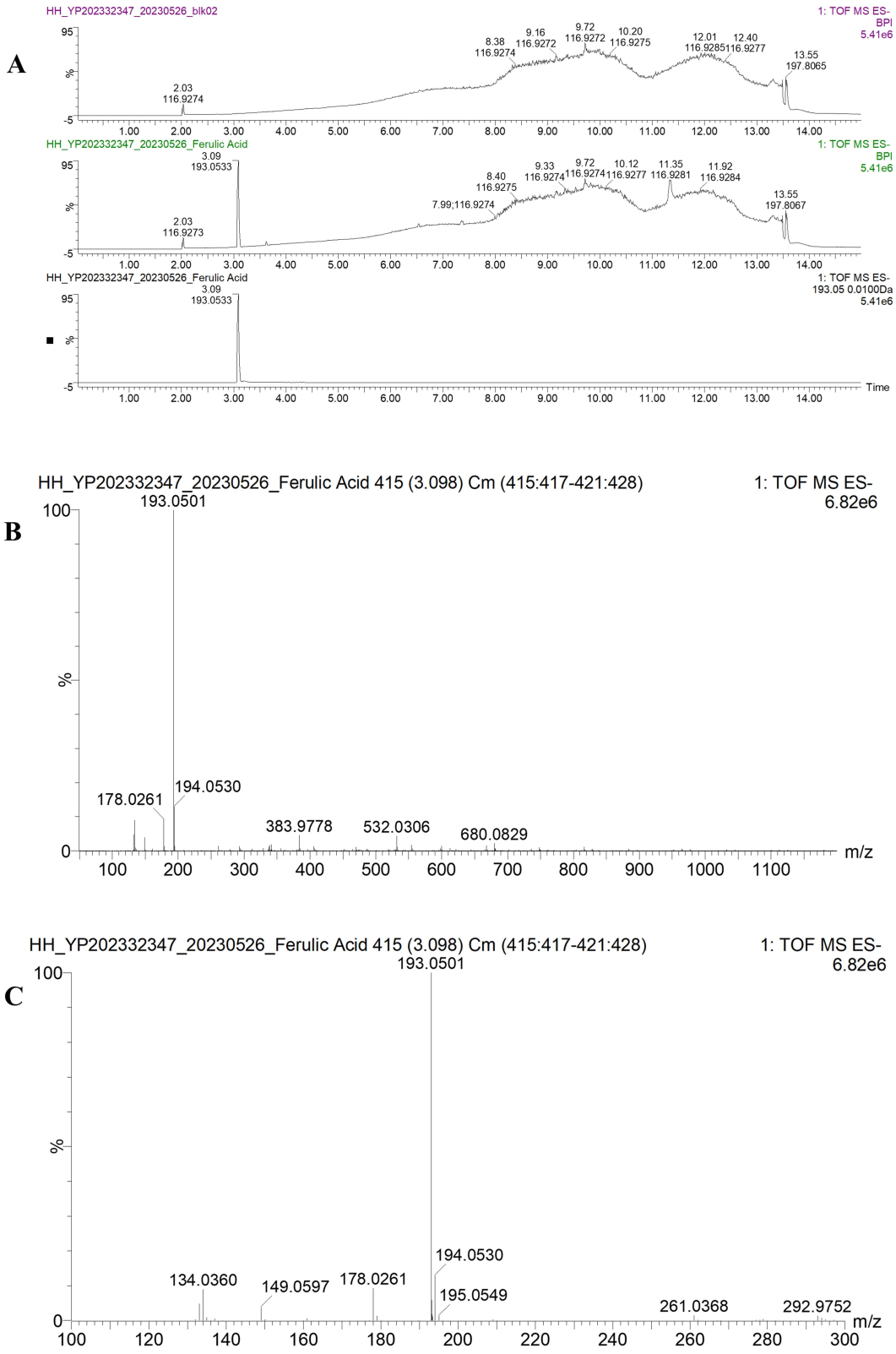

Figure 4 UPLC-MS analysis of the FA. (**A**) Representative chromatograms showing: base peak ion chromatogram of blank control (upper panel), base peak ion chromatogram of sample (middle panel), and extracted ion chromatogram at m/z 193.0501 (lower panel). (**B**) Full-scan mass spectrum (m/z 50–1200) of the sample at retention time 3.09 min. (**C**) Zoomed mass spectrum (m/z 100–300) of the sample at retention time 3.09 min.

https://doi.org/10.2147/NSA.S500407

Table 8 Mass Spectrometric Analysis Data of Ferulic Acid-Loaded Lipid Nanoparticles (FA-LNPs)

Mass	Calc. Mass	mDa	PPM	DBE	i-FIT	Norm	Conf (%)	Formula
193.0501	193.0501	0.0	0.0	6.5	284.4	0.052	94.97	C10H9O4

considerations include: Enhanced cellular uptake and tissue penetration, potential interaction with biological barriers, biodistribution and clearance patterns, and cellular internalization mechanisms.

Acute Toxicity Study of Intravenously Administered FA Nanoparticles in SD Rats

This comprehensive study evaluated the extended acute toxicity and pharmacokinetics of FA-LNPs following intravenous administration, providing crucial evidence for their potential clinical application.

Cage-Side Observations

During the study period, one female animal in the 200 μg/kg LPS group was found dead on the second day post-administration. Similarly, apart from the deceased animals, no notable abnormalities were observed during cage-side observations of male and female animals in the blank control group, Con-LNPs group, in the 200 μg/kg LPS group, both male and female animals exhibited hunched posture and piloerection (Supplementary Table 01: Individual Data for Paraventricular Observation).

Body Weight

During the study period, compared to the concurrent same-sex blank control group, male animals in the 200 μg/kg LPS group exhibited a significant decrease in body weight from day 2 to day 6 ($P \leq 0.05$ or 0.01), No consistent or statistically significant changes in body weight were observed in animals from the other dose groups (Supplementary Table 02: Body Weight Statistical Data).

Food and Water Consumption

During the study period, compared to the concurrent same-sex blank control group, both male and female animals in the positive control group (LPS 200 μg/kg) exhibited reduced food and water consumption on days 1~2. These parameters returned to levels comparable to the blank control group by day 3 of the recovery period (Supplementary Table 03: Food Consumption Statistical Data; Supplementary Table 04: Water Intake Statistical Data).

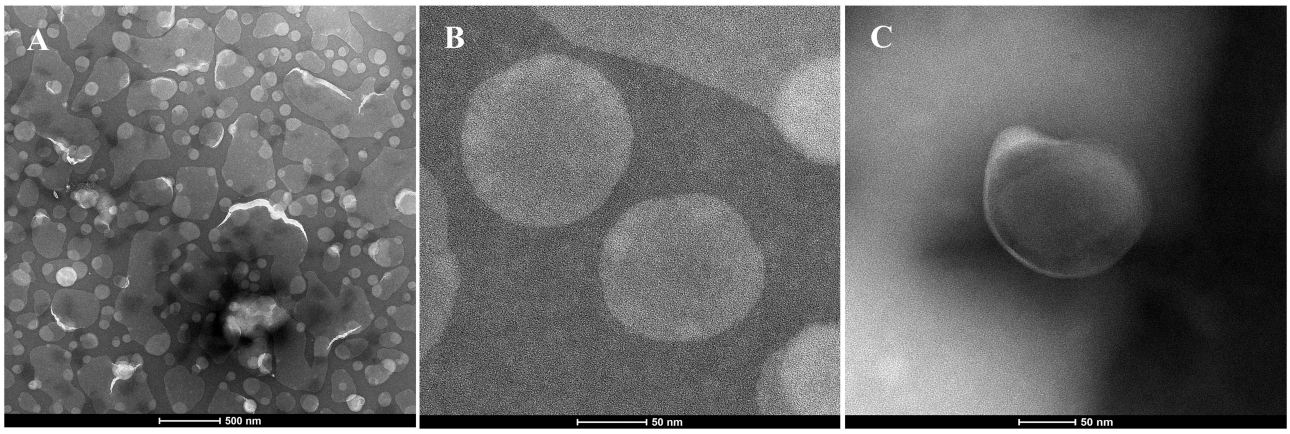

Figure 5 Transmission electron microscopy (TEM) characterization of ferulic acid-loaded liposomal nanoparticles (FA-LNPs). (**A**–**C**) Representative TEM micrographs at different magnifications showing spherical FA-LNPs with an average diameter of 80 nm. Samples were prepared by 3-fold dilution in phosphate buffer (pH 7.4). Scale bars: 500 nm and 50nm.

Size Distribution Report by Intensity

v2.2

Malvern

Sample Details

Sample Name: 6-2-10mg 1

SOP Name: size measurement.sop

General Notes:

File Name:	Huanghhao.dts	**Dispersant Name:**	Water
Record Number:	25	**Dispersant RI:**	1.330
Material RI:	1.59	**Viscosity (cP):**	0.8872
Material Absorbtion:	0.010	**Measurement Date and Time:**	June 2, 2023. 11:10:39

System

Temperature (°C):	25.0	**Duration Used (s):**	60
Count Rate (kcps):	339.8	**Measurement Position (mm):**	4.65
Cell Description:	Disposable sizing cuvette	**Attenuator:**	11

Results

			Size (d.n...	% Intensity:	St Dev (d.n...
Z-Average (d.nm):	83.85	**Peak 1:**	89.37	100.0	23.22
PdI:	0.053	**Peak 2:**	0.000	0.0	0.000
Intercept:	0.954	**Peak 3:**	0.000	0.0	0.000

Result Good

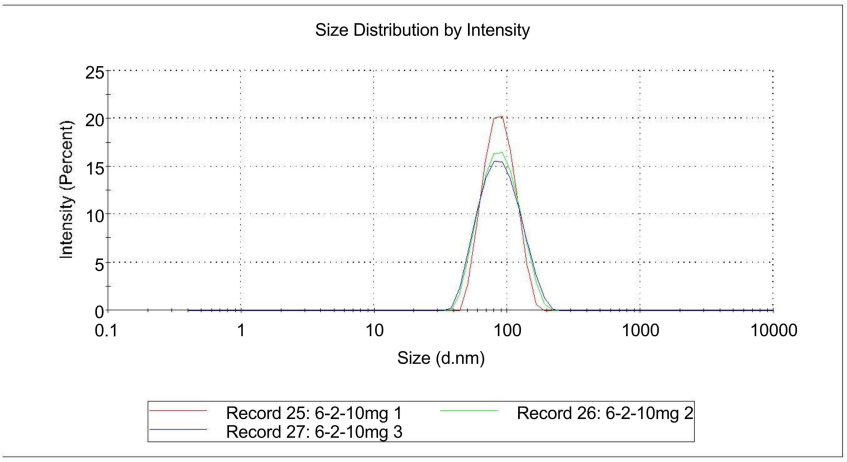

Malvern Panalytical
www.malvernpanalytical.com

Zetasizer Ver. 8.00.4813
Serial Number : MAL1166268

File name: HuangHao.dts
Record Number: 25
June 2, 2023 13:14:13

Figure 6 Dynamic Light Scattering (DLS) measurements of Ferulic Acid. The ferulic acid-loaded liposomes exhibited an increased hydrodynamic diameter compared to empty liposomes, with an approximate increase of 10 nm in saline and 5 nm in Tris buffer. The FA liposome nanoparticles synthesized using the microfluidic device demonstrated remarkable uniformity in size distribution, characterized by a Z-Average diameter of 83.85 nm and a low polydispersity index (PDI) of 0.053.

https://doi.org/10.2147/NSA.S500407

Zeta Potential - Quality

Malvern Panalytical

Sample Details

Sample Name:	231129-1-zeta		
Project Name:	Project 1		
Date and Time:	2023/11/29 13:49:03		
Type:	Zeta	Result Source:	Instrument
Cell Name:	DTS1070	Temperature (°C):	25
Material Name:	Polystyrene latex	Dispersant Name:	Water
Material RI:	1.59	Dispersant RI:	1.33
Material Absorption:	0.01	Dispersant Viscosity (cP):	0.887
		Dispersant Dielectric Constant:	78.5

Zeta Potential Distribution

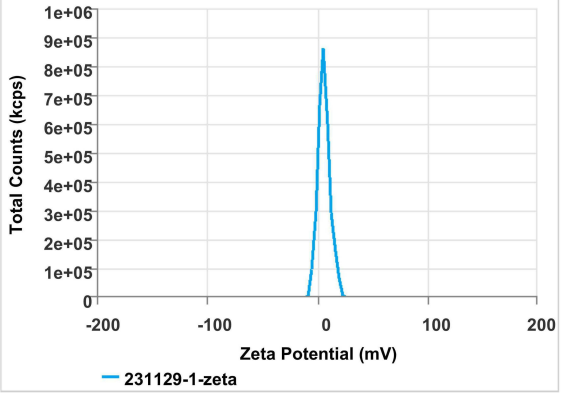

Phase Plot

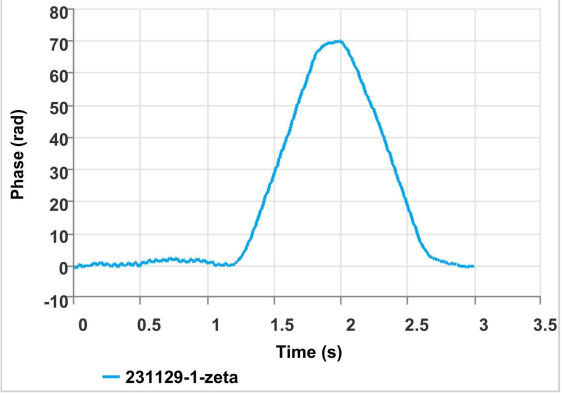

Statistics Table

Name	Mean	Standard Deviation	RSD	Minimum	Maximum
Zeta Potential (mV)	5.969	-	-	5.969	5.969
Zeta Peak 1 Mean (mV)	5.969	-	-	5.969	5.969
Conductivity (mS/cm)	0.0128	-	-	0.0128	0.0128
Wall Zeta Potential (mV)	14.31	-	-	14.31	14.31
Zeta Deviation (mV)	5.444	-	-	5.444	5.444
Derived Mean Count Rate (kcps)	3.71E+04	-	-	3.71E+04	3.71E+04
Reference Beam Count Rate (kcps)	2861	-	-	2861	2861
Quality Factor	1.701	-	-	1.701	1.701

Parameter List

Actual Instrument Settings\Instrument Serial Number : MAL1310599

Software Version : 3.3.0.42

ZS XPLORER

Malvern Panalytical Ltd.
www.malvernpanalytical.com

ZS XPLORER
Page 1 of 1

Template Created: 2019/5/14
Printed: 2025/2/7 15:36

Figure 7 Zeta potential and stability analysis of FA-LNPs. Zeta potential distribution of FA-LNPs, showing a mean value of +5.969 mV, indicating moderate colloidal stability. Stability profile of FA-LNPs over two weeks, demonstrating no significant changes in particle size or polydispersity index (PDI). The optimized preparation process and unique surface properties contribute to the excellent stability of the nanoparticle formulation.

Table 9 Physicochemical Characteristics of FA-Loaded Liposomes Prepared by Thin-Film Hydration Method

Batch No.	Concentration (mg/mL)	Concentration (mg/mL)	Particle Size (nm)	PDI
230826-1	3.10	66.92	328	0.687

Table 10 Physicochemical Characteristics of FA-Loaded Liposomes Prepared by Aqueous Method

Batch No.	Concentration (mg/mL)	Concentration (mg/mL)	Particle Size (nm)	PDI
230826-3	0.43	53.10	260.4	0.357

Table 11 Characterization of FA-Loaded Liposomes Prepared by Active Loading Method Across Multiple Batches (230826–2 to 230826–9)

Batch No.	Concentration (mg/mL)	Concentration (mg/mL)	Particle Size (nm)	PDI
230826-2	4.81	37.21	141.4	0.039
230826-2-2	4.80	45.09	Not detected	
230826-4	0.43	53.10	143.2	0.04
230826-5	3.56	61.82	182.9	0.212
230826-6	3.51	52.09	144.1	0.081
230826-7	4.38	59.31	143.1	0.056
230826-8	3.98	52.00	Not detected	
230826-9	2.94	59.06	167.6	0.178

Table 12 Physicochemical Characterization of FA-Loaded Liposomal Nanoparticles

Parameter	Method	Result
Drug content	HPLC	4.65 mg/mL
Encapsulation efficiency	Ultrafiltration centrifugation-HPLC	86.35%
Mean particle size	Dynamic light scattering	d=128.9 nm
Polydispersity index (PDI)	Dynamic light scattering	0.018

Table 13 Physicochemical Characterization of Blank Liposome Nanoparticles

Parameter	Method	Result
Mean particle size	Dynamic light scattering	d=128.9 nm
Polydispersity index (PDI)	Dynamic light scattering	0.018

Clinical Pathology Examination

At the end of the observation period (D7), male animals in the vehicle control group showed decreased reticulocyte count and percentage. The positive control group (LPS 200 μg/kg) demonstrated elevated PLT, PCT, UA, and K levels, with decreased MCH. Female animals in the FA-LNPs group exhibited increased MPV (Supplementary Table 05: Hematology Statistical Data; Supplementary Table 06: Serum Biochemistry Statistical Data).

Organ Weight

At the end of the observation period (D7), compared to the concurrent same-sex blank control group, male animals in both the vehicle control (Co-LNPs group) and positive control (LPS 200 μg/kg) groups showed statistically significant decreases in heart weight ($P \leq 0.05$ or 0.001). No notable abnormalities were observed in organ coefficients (Supplementary Table 07: Organ Weight Statistical Data).

Gross Necropsy Observations

Male animal No. 43 in the LPS 200 μg/kg group exhibited bilateral yellow discoloration of the kidneys. No other apparent macroscopic lesions were observed.

Pharmacokinetic Parameters

Following intravenous administration of FA-LNPs at 46.5 mg/kg, the C_{max} of FA in male and female SD rats was 420,000 ± 29,513 and 318,667 ± 86,639 ng/mL, respectively. The AUC_{0-t} values were 80,414 ± 10,778 and 93,885 ± 13,429 h*ng/mL for males and females, respectively, with no significant gender differences observed (Table 14).

The mean residence time (MRT_{0-t}) was 2.83 ± 0.792 h, while the elimination half-life ($t_{1/2}$) was 12.8 ± 1.88 h. The systemic clearance (CLz/F) was 0.535 ± 0.0851 L/h/kg. The discrepancy between MRT and t1/2 suggests that FA nanoparticles may follow a multi-compartment model in SD rats, with the terminal elimination half-life (t1/2β) being substantially longer than the MRT.

The apparent volume of distribution (Vz) was 9.73 ± 1.25 L/kg, indicating that the drug is primarily distributed in plasma and extracellular fluid, with limited penetration across cell membranes (Table 15).

Pathological and Neurotoxicity Assessment

This study aimed to evaluate the neurotoxicity of FA liposome nanoparticles (FA-LNPs) and preliminarily explore their intervention effects on lipopolysaccharide (LPS)-induced neurological damage. Our findings reveal the complex role of FA-LNPs in an LPS-induced neuroinflammation model and their potential neuroprotective properties.

Histopathological analysis indicated no significant abnormalities in major organs (liver, kidney, heart, and brain) following FA-LNPs administration alone. See Figure 8A. However, LPS injection induced a systemic inflammatory response, leading to pathological changes in multiple organs, particularly the liver and heart, See Figure 8B–E.

Regarding the nervous system, H&E (Figure 8F) and Luxol Fast Blue staining (Figure 9) showed no apparent abnormalities in brain tissue structure or cellular morphology across control, LPS, and LPS+FA-LNPs groups. Nevertheless, immunohistochemistry analyses revealed significant LPS-induced neuroinflammatory responses.

Table 14 The Ratio of C_{max} and AUC_{0-t} of FA Between Different Gender Groups

Dose			**46.5 mg/kg**	
Sex			**Female**	**Male**
C_{max}	ng/mL	Mean	318667	420000
		Ratio	1	1.318
AUC_{0-t}	h*ng/mL	Mean	93885	80414
		Ratio	1	0.857

Table 15 Main Pharmacokinetic Parameters of FA in SD Rats After Intravenous Administration

Dose		46.5 mg/kg	
Sex		**Female**	**Male**
AUC0-t	h*ng/mL	93885±13429	80414±10778
AUC0-∞	h*ng/mL	95361±13799	81957±11959
MRT0-t	h	2.80±0.676	2.87±1.05
MRT0-∞	h	3.77±1.05	4.02±2.06
t1/2	h	12.9±1.37	12.6±2.62
Tmax	h	0.0167±0.00	0.0167±0.00
CLz/F	L/h/kg	0.495±0.0746	0.576±0.0875
Vz	L/kg	9.12±0.828	10.3±1.45
Cmax	ng/mL	318667±86639	420000±29513
C0	ng/mL	363472±105864	529000±35283

GFAP staining results demonstrated a significant increase in astrocyte activation in the LPS group compared to the control group ($p < 0.01$), indicating successful induction of neuroinflammation, Interestingly, the LPS+FA-LNPs group showed no significant difference in GFAP expression levels compared to the LPS group ($p > 0.05$). This finding suggests that FA-LNPs did not significantly inhibit LPS-induced astrocyte activation under the experimental conditions of this study. See Figure 10A and B.

Similarly, IBA-1 staining results showed significant microglial activation by LPS ($p < 0.05$), while FA-LNP treatment failed to effectively suppress this activation in the short term ($p > 0.05$). However, this discrepancy may be attributed to factors such as short treatment duration, dosing regimen, or bioavailability of FA-LNPs (Figure 11A and B). Fluoro-Jade staining further confirmed LPS-induced neurodegenerative changes ($p < 0.05$). Notably, despite intervention with FA-LNPs, the treatment group exhibited a subtle but concerning trend of exacerbated neurodegenerative changes compared to the LPS group, albeit without achieving statistical significance ($p < 0.05$). This unexpected observation suggests not only an absence of neuroprotective effects but potentially a marginally detrimental impact of FA-LNPs on neurodegeneration (Figure 12A and B). These findings underscore the critical importance of rigorously evaluating nanomaterial-based interventions and caution against presumptive neuroprotective strategies.

Network Pharmacology Analysis of Ferulic Acid

To explore the potential mechanisms of FA in treating multiple diseases (Alzheimer's disease, COPD, acute exacerbation of COPD, and atherosclerosis), a comprehensive network pharmacology analysis was performed. Utilizing SwissTargetPrediction and Super-PRED databases, 176 potential FA targets were identified. Disease-related targets (n=47,043) were collected from GeneCards, OMIM, CTD, and DisGenet databases. Venn diagram analysis revealed 141 common targets between FA and disease targets (Figure 13A).

A compound-disease-target network was constructed using Cytoscape 3.9.0, illustrating the multi-target therapeutic potential of FA. The protein-protein interaction (PPI) network, generated via STRING database, comprised 141 nodes and 794 edges (average degree=11.3), see Figure 13B and C. Five hub targets were identified based on degree values: EGFR, ESR1, PTGS2, CTNNB1, and STAT3, suggesting their crucial roles in FA's therapeutic effects[32,33] (Table 16).

GO enrichment analysis revealed 504 terms (59 cellular components, 324 biological processes, and 121 molecular functions). The targets were mainly enriched in plasma membrane, cytoplasm, and transcription factor complexes, with critical processes including single-carbon metabolism, exogenous stimuli response, and β-amyloid cellular response.

https://doi.org/10.2147/NSA.S500407

KEGG pathway analysis identified 118 significantly enriched pathways ($p<0.05$), notably nitrogen metabolism, AGE-RAGE signaling, and ROS-related chemical carcinogenesis.[34,35] See Figure 13D and E.

Molecular docking analysis demonstrated favorable binding affinities between FA and the five key targets (Table 17), with binding energies ranging from −7.6 kcal/mol (PTGS2) to −5.2 kcal/mol (CTNNB1), see Figure 14. These findings collectively suggest FA's multi-target therapeutic potential through regulation of diverse biological pathways.[36]

Discussion

Ferulic Acid Attenuates LPS-Induced Neuroinflammation and Associated Behavioral Deficits

Inflammation is one major causative factor associated with several age-related and chronic diseases, such as AD and diabetes.[37,38] It is widely recognized that oxidative stress has a key role to be implicated in the onset and progression of many different pathologies, among which neurodegenerative diseases and metabolic ailments.[39] Among phenolic acids, FA has recently been proposed as a potential neuroprotective agent. Indeed, it seems to ameliorate AD pathology by

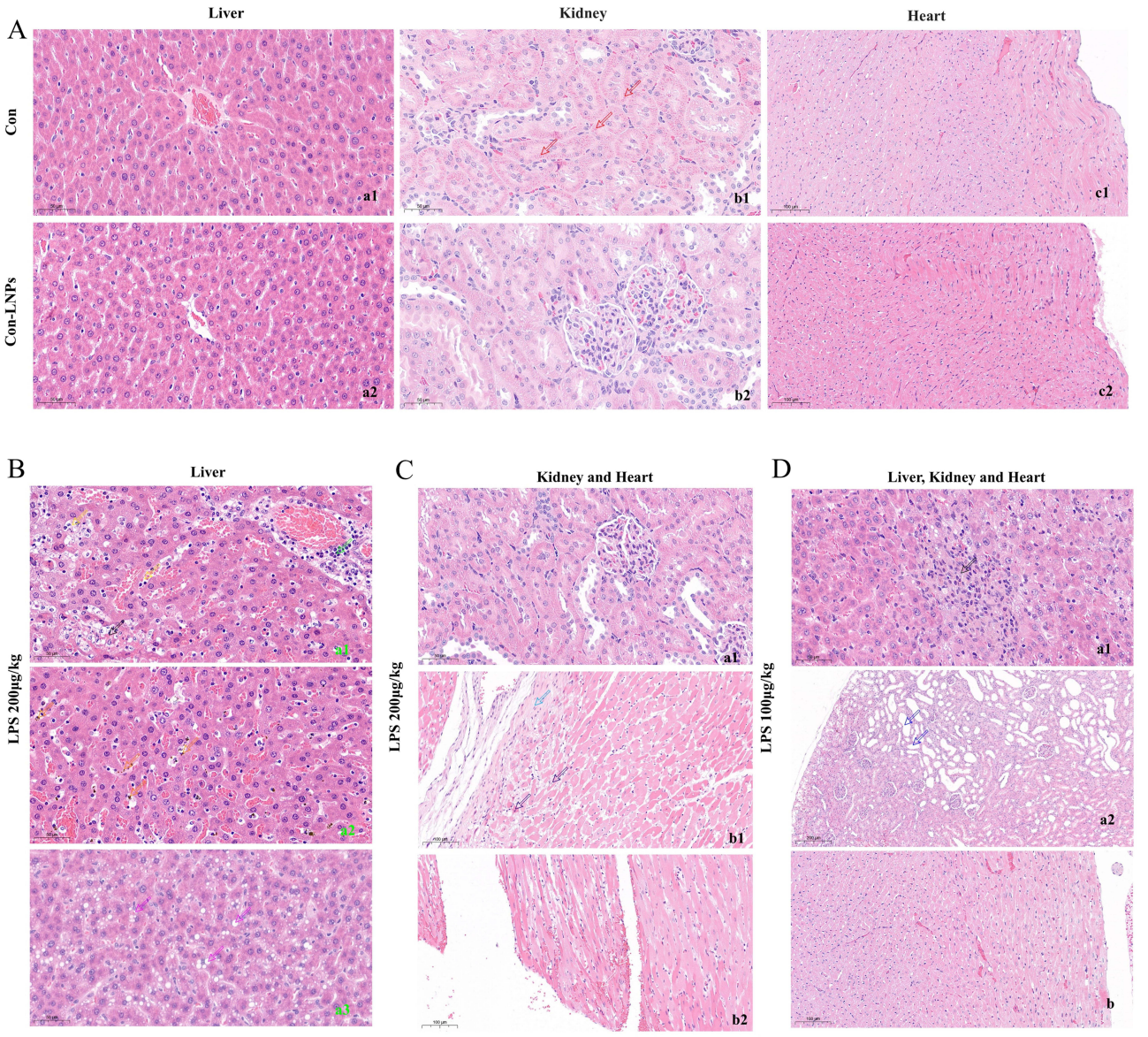

Figure 8 Continued.

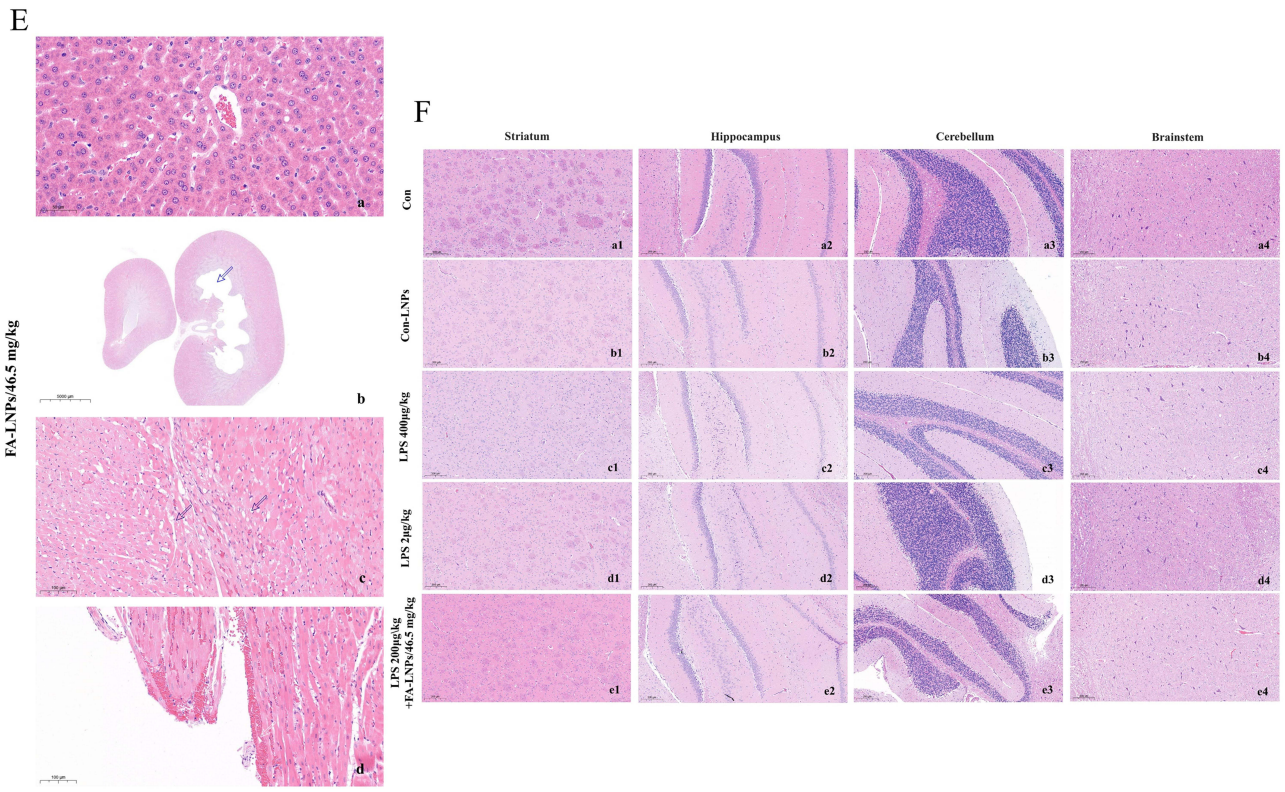

Figure 8 Histopathological examination of major organs in rats across different treatment groups. (**A**) Representative histopathological images of major organs in control groups (H&E staining). (a1-c1) Blank control group: normal liver architecture with intact lobular structure and hepatic cords (a1); kidney showing clear cortical and medullary structures, with one animal exhibiting mild, diffuse hyaline droplet accumulation in renal tubules (b1); and normal cardiac tissue with well-preserved endocardium, myocardium, and epicardium (c1). (a2-c2) Vehicle control group (Con-LNPs): liver displaying normal architecture without pathological changes (a2); kidney with clear demarcation of cortical and medullary regions and no apparent abnormalities (b2); and heart tissue showing normal myocardial structure with distinct cardiomyocytes and intercalated discs (c2). Scale bar = 50 μm or 100 μm. (**B**) Representative histopathological changes in liver tissues of rats in LPS 200 μg/kg group. (a1) Liver section showing mild congestion (white arrow), increased sinusoidal cells (yellow arrow), mononuclear cell infiltration in the confluent area (green arrow), and focal hepatocellular necrosis with inflammatory cell infiltration (black arrow). (a2) Liver section demonstrating pigment deposition (Orange arrow) in Kupffer cells and hepatocytes. (a3) Liver section exhibiting hepatocellular vacuolation (purple arrow). Scale bars = 50 μm. H&E staining. (**C**). Representative histopathological changes in kidney and heart tissues of rats in LPS 200 μg/kg group. (a1) Kidney section showing normal renal architecture with well-preserved cortical and medullary structures, intact glomeruli and tubules (40× magnification). (b1) Heart section exhibiting multifocal myocardial alterations, including focal fibrosis with fibroblast proliferation and collagen deposition (light blue arrow), myocardial degeneration/necrosis characterized by widened interstitium, myofibril dissolution, increased cytoplasmic eosinophilia, and nuclear pyknosis (dark blue arrow), and myocardial hemorrhage (white arrow) (20× magnification). (b2) Higher magnification view of heart section from animal No. 16 showing detailed myocardial fibrosis and degeneration/necrosis (20× magnification). Note: Kidney tissue from animal No. 16 was excluded due to autolysis. Scale bars = 100 μm (b1, b2) and 50 μm (a1). H&E staining. (**D**) Representative histopathological changes in liver, kidney, and heart tissues of rats in LPS 100 μg/kg group. (a1) Liver section showing mild multifocal hepatocellular necrosis with inflammatory cell infiltration (black arrow), characterized by focal destruction of hepatic cords and inflammatory cell infiltration (40× magnification). (a2) Kidney section exhibiting mild multifocal tubular dilation (blue arrow), with preserved cortical and medullary structures and intact glomeruli (10× magnification). (b) Heart section from animal No. 43 displaying normal cardiac architecture with intact endocardium, myocardium, and epicardium, showing no significant pathological changes (20× magnification). Scale bars = 50 μm (a1), 200 μm (a2), 100 μm (a3) H&E staining. (**E**) Representative histopathological examination of major organs from rats treated with FA-LNPs (46.5 mg/kg × 2) for 7 days. (a) Liver section showing normal hepatic architecture without pathological changes (40× magnification). (b) Kidney section demonstrating moderate renal pelvic dilation (blue arrow) (6× magnification). (c, d) Heart sections exhibiting mild, multifocal myocardial degeneration/necrosis characterized by slightly widened interstitium, myofibril dissolution, and cytoplasmic vacuolation (dark blue arrow) (c), and mild, multifocal myocardial hemorrhage (white arrow) (d) (both at 20× magnification). Scale bars = 50 μm (a), 5000 μm (b), and 100 μm (c, d). H&E staining. FA-LNPs: ferulic acid -modified liposome nanoparticles. (**F**) Representative histopathological examination of brain tissues from rats across different treatment groups. (a1-e4) Photomicrographs showing striatum (a1-e1), hippocampus (a2-e2), cerebellum (a3-e3), and brainstem (a4-e4) from rats treated with: blank control group (a1-a4), Con-LNPs group (b1-b4), LPS 200 μg/kg group (c1-c4), LPS 100 μg/kg group (d1-d4), and FA-LNPs (46.5 mg/kg × 2) (e1-e4). All brain regions displayed normal architecture across treatment groups, with preserved cellular morphology in cerebral cortex, and no evidence of cellular disarray, apoptosis, hemorrhage, or inflammatory responses in the striatum, hippocampus, cerebellum, and brainstem. Note: Brain tissue from animal No. 16 in the high-dose LPS group was excluded due to autolysis. All images were taken at 100× magnification. Scale bars = 100 μm. H&E staining.

Abbreviations: LNPs, liposome nanoparticles; LPS, lipopolysaccharide; FA-LNPs, ferulic acid-modified liposome nanoparticles.

preventing neurodegeneration in several brain regions; FA has been shown to inhibit Aβ oligomer aggregations, against Aβ(1–42) toxicity and to exert antioxidant, anti-inflammatory, and anti-apoptotic effects.[40–42]

FA treatment interfered with the TLR4/MD2 complex binding site, a down-regulation by FA of nitric oxide synthase (iNOS), cyclooxygenase-2 (COX-2), TNF-α, IL-1β, has been observed following NF-κB inhibition in LPS-treated mice.[43] LPS also be used for hypoxia stimulation, in a mouse high-altitude cerebral edema model. Keli Yao et al

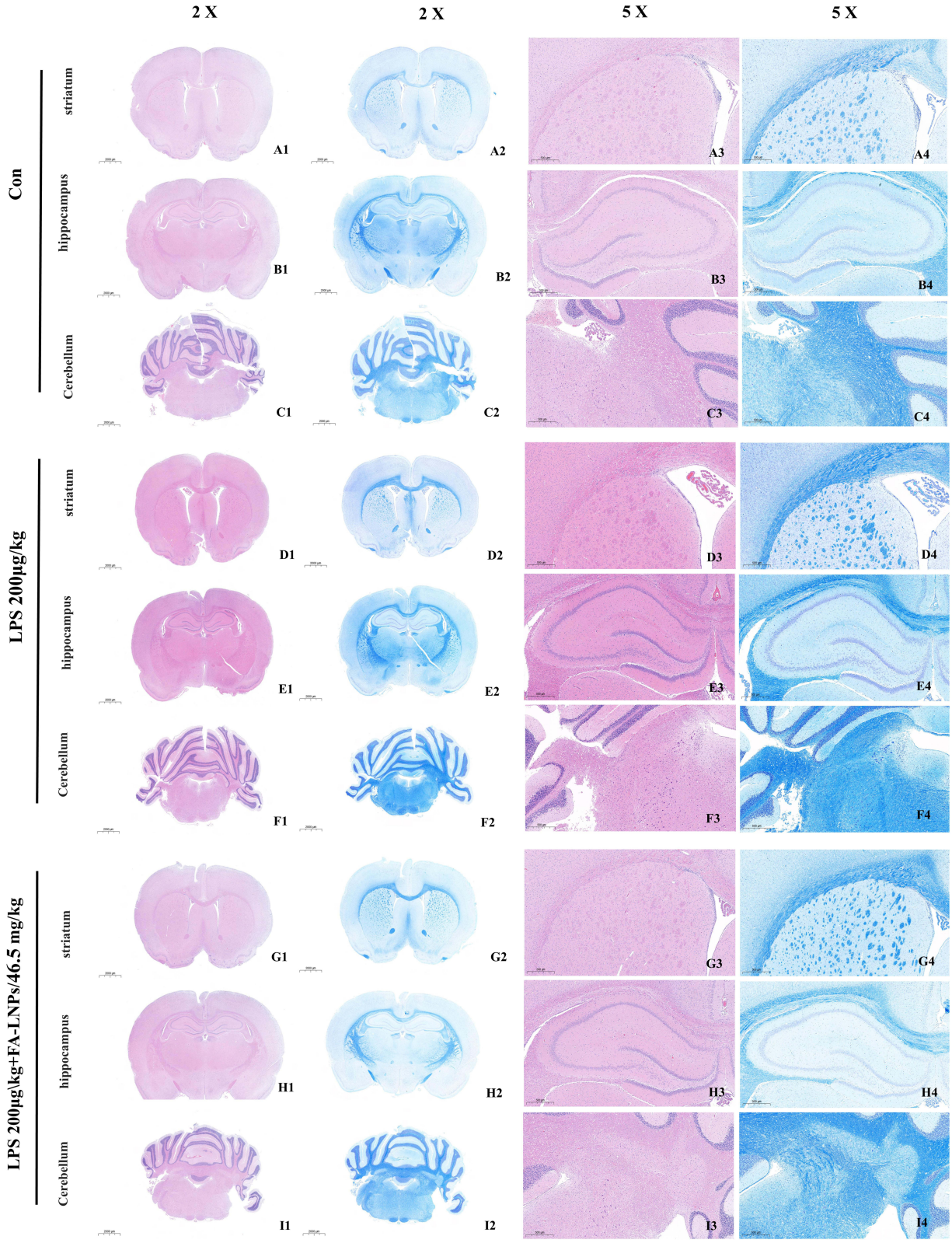

Figure 9 Histopathological analysis of rat brain tissues following repeated intravenous administration of FA liposome nanoparticles (FA-LNPs). Representative images of brain sections from (A1-C4) control group, (D1-F4) LPS group (200 μg/kg), and (G1-I4) LPS + FA-LNPs group (200 μg/kg LPS + 46.5 mg/kg FA-LNPs). No significant histopathological changes were observed across all groups. H&E staining revealed normal brain structure with intact meninges, cortical layers, and white matter. LFB staining showed no evidence of demyelination in any group. There was no perivascular cuffing or meningeal infiltration of lymphocytes and macrophages observed in any of the examined sections. This comprehensive histopathological analysis suggests that repeated intravenous administration of FA-LNPs does not induce detectable neuropathological changes in rat brain tissues, even in the presence of LPS-induced inflammation.

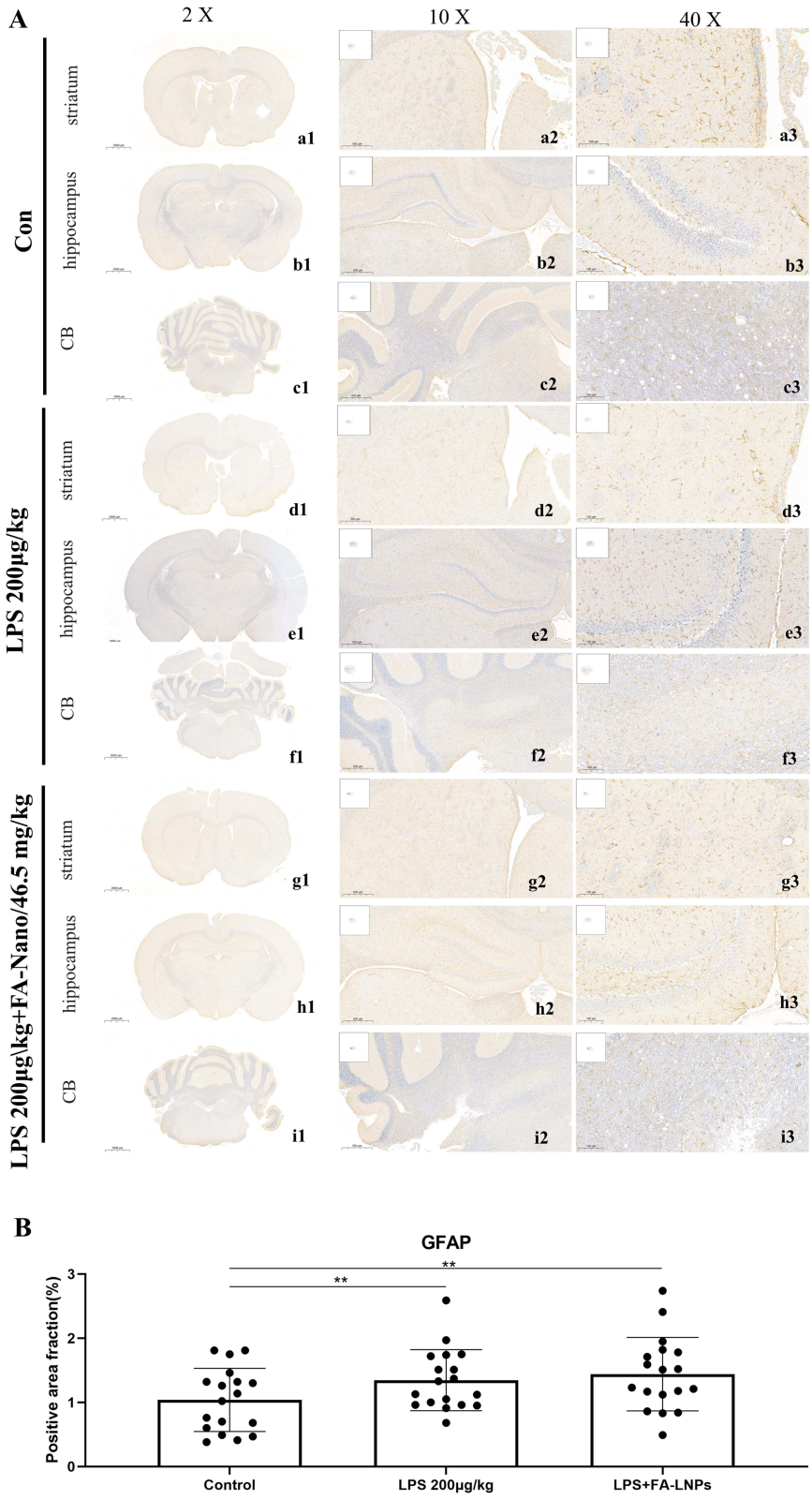

Figure 10 GFAP immunostaining analysis and quantitative assessment of astrocyte activation in rat brain tissues. (**A**) GFAP immunostaining analysis of astrocyte activation in rat brain tissues. (a1-i3) Representative images of GFAP immunostaining in the control, LPS (200 μg/kg), and LPS+FA-LNPs (200 μg/kg LPS + 46.5 mg/kg FA-LNPs) groups. Scale bar: 2000 μm (2×), 500 μm (10×) and 100 μm (40×). (**B**) Quantification of GFAP-positive area ratio (GFAP-positive area / total brain tissue area) across different treatment groups. Data are presented as mean ± SEM. **p < 0.01 compared to the control group. ns: not significant compared to the LPS group. n = 6 per group. GFAP staining revealed significant astrocyte activation in the LPS group compared to the control ($p < 0.01$), indicating successful induction of neuroinflammation. The LPS+FA-LNPs group showed no significant difference in GFAP expression compared to the LPS group ($p > 0.05$), suggesting that FA-LNPs did not significantly inhibit LPS-induced astrocyte activation under these experimental conditions. Images were captured at 400× magnification using a 3DHISTECH P250 scanner and analyzed with Quant Center software.

https://doi.org/10.2147/NSA.S500407

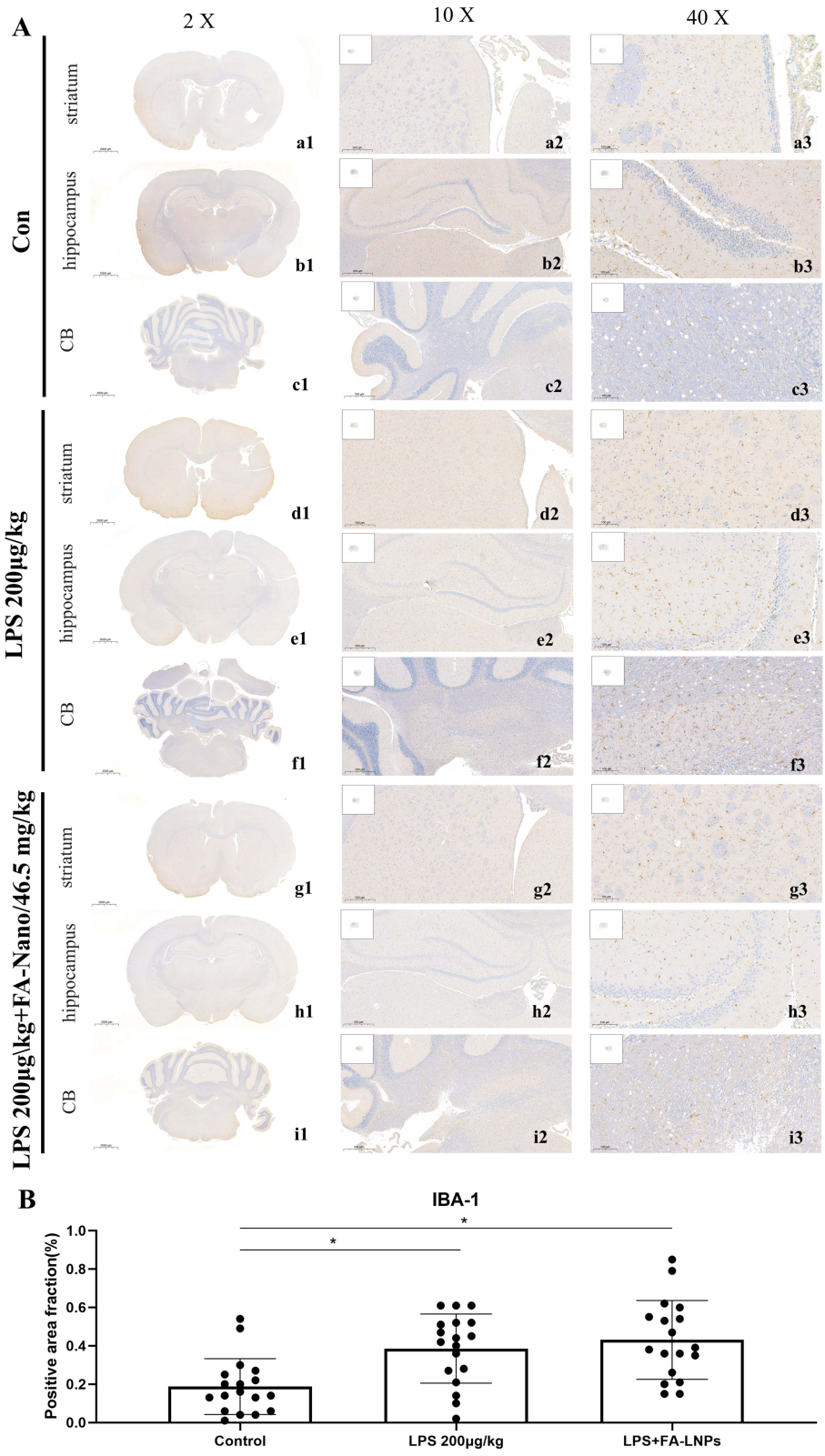

Figure 11 Evaluation of FA-LNPs on LPS-Induced microglial activation in rat brain using Iba-1 immunostaining analysis. (**A**) Iba-1 immunostaining analysis of microglial activation in rat brain tissues. (a1-i3) Representative images of Iba-1 immunostaining in the control, LPS (200 μg/kg), and LPS+FA-LNPs (200 μg/kg LPS + 46.5 mg/kg FA-LNPs) groups. Scale bar: Scale bar: 2000 μm (2×), 500 μm (10×) and 100 μm (40×). (**B**) Quantification of Iba-1-positive area ratio (Iba-1-positive area / total brain tissue area) across different treatment groups. Quantification of Iba-1-positive cell ratio (number of Iba-1-positive cells / total number of brain cells) across different treatment groups. Data are presented as mean ± SEM. *$p < 0.05$ compared to the control group. n = 6 per group. Iba-1 staining demonstrated significant microglial activation in the LPS group compared to the control ($p < 0.05$). FA-LNPs treatment did not effectively suppress this activation in the short term ($p > 0.05$), as evidenced by both area ratio and cell ratio analyses. Images were captured at 400× magnification using a 3DHISTECH P250 scanner and analyzed with Quant Center software.

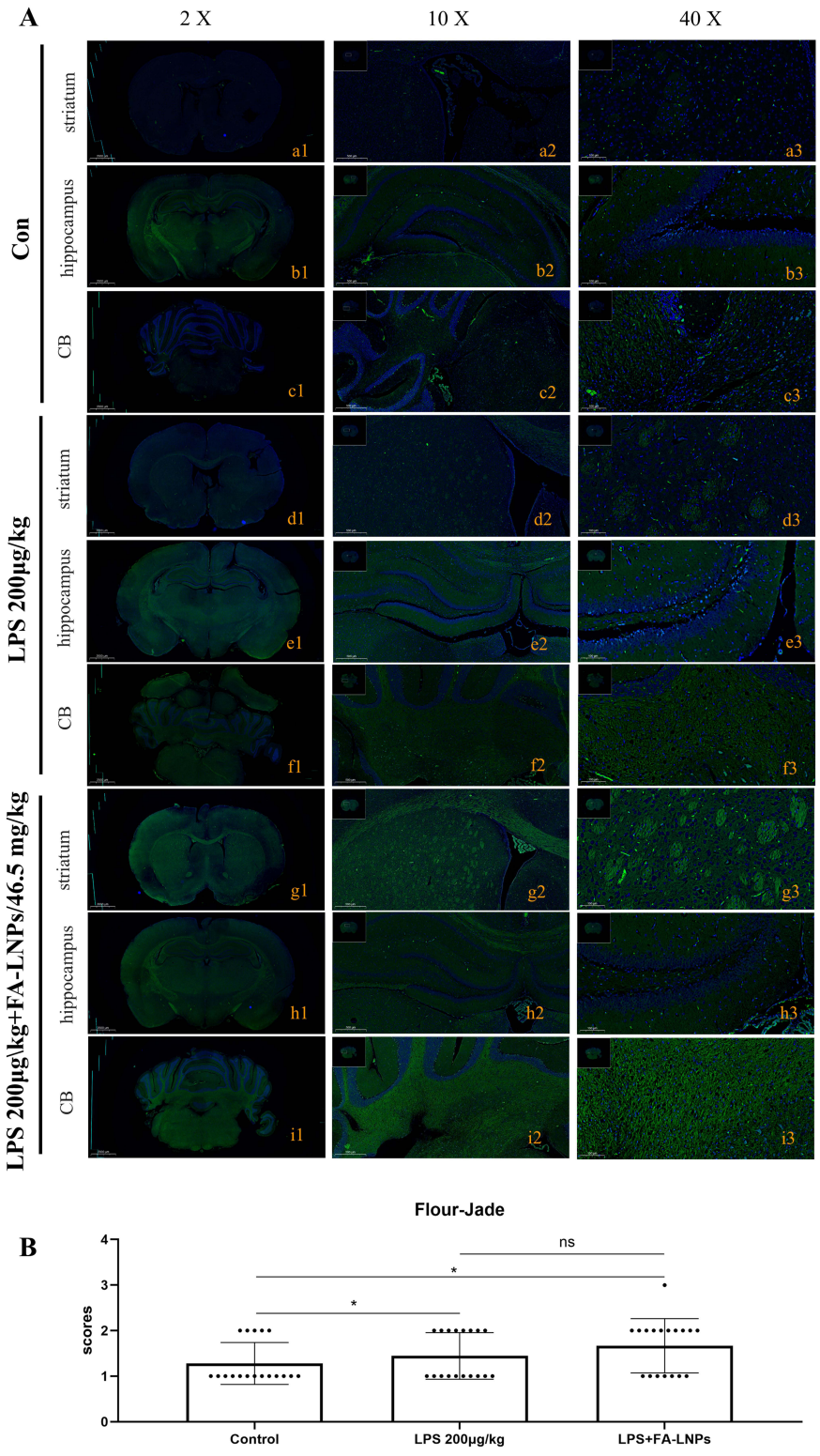

Figure 12 Fluoro-Jade B (FJB) staining showing neurodegeneration in rat brain tissues following LPS and FA-LNP treatments. (**A**) Representative images of FJB staining in rat brain tissues. Scale bar: 2000 μm (2×), 500 μm (10×) and 100 μm (40×). (**B**) Quantification of FJB-positive neurons using a semi-quantitative scoring system. Bars represent mean ± SEM (n = 6 per group). *p < 0.05 compared to control group; ns: not significant compared to LPS group (one-way ANOVA followed by Tukey's post-hoc test). FJB staining was performed to evaluate neuronal degeneration. Deparaffinized and rehydrated sections were incubated with FJB working solution overnight at 4°C, counterstained with DAPI, and coverslipped. Images were acquired using a Pannoramic 250 slide scanner. FJB-positive neurons were scored using a 5-point scale (0–4) based on the percentage of stained neurons, where 0 indicates no neuropathology and 4 indicates severe neuropathology (>45% of neurons stained). LPS treatment significantly increased FJB-positive neurons compared to the control group (*p < 0.05), indicating enhanced neurodegeneration. FA-LNPs treatment showed no significant difference compared to the LPS group (ns, p > 0.05), suggesting that FA-LNP treatment did not effectively attenuate LPS-induced neurodegeneration.

https://doi.org/10.2147/NSA.S500407

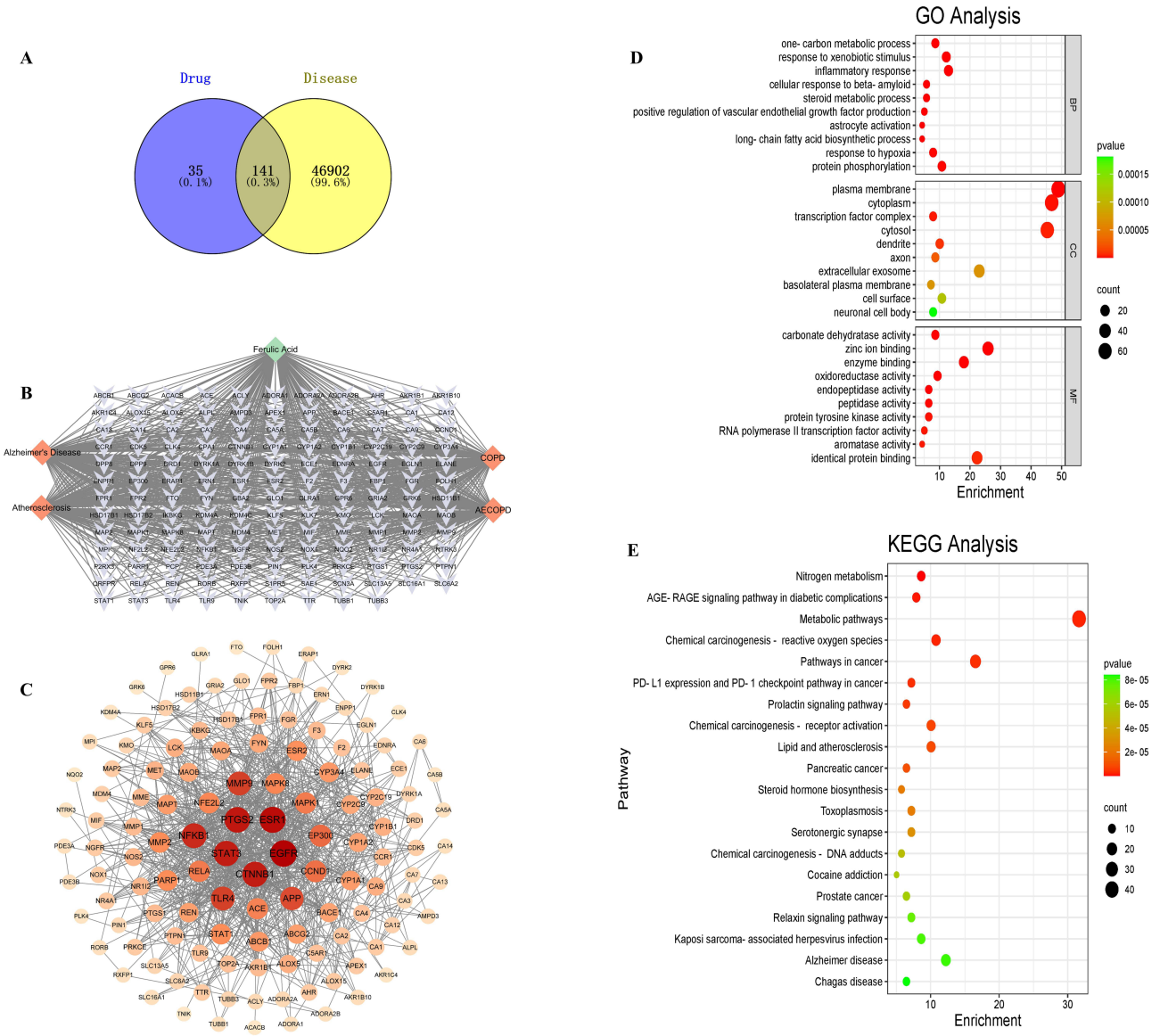

Figure 13 Network pharmacology analysis revealing the potential mechanisms of FA. (**A**) Venn diagram illustrating the overlap between FA targets and disease-related genes. (**B**) Compound-disease-target network analysis showing the interactions between FA (green diamond), diseases (red diamonds), common targets (purple triangles), and specific targets (grey circles). (**C**) Protein-protein interaction (PPI) network of common targets consisting of 141 nodes and 794 edges, where node size represents degree value and edge thickness indicates interaction confidence score (minimum required score = 0.400). (**D**) Top 10 significantly enriched Gene Ontology (GO) terms ($p<0.05$, $q<0.05$) across biological process (BP), cellular component (CC), and molecular function (MF) categories. Bar length represents -log10(p-value), color intensity indicates significance level, and bar width shows gene count. (**E**) Top 20 significantly enriched KEGG pathways ($p<0.05$), highlighting key pathways including nitrogen metabolism, AGE-RAGE signaling, metabolic pathways, and ROS-related chemical carcinogenesis. Bar representation follows the same format as in (D).
Abbreviations: FA, ferulic acid; AGE-RAGE, advanced glycation end products-receptor for AGE; ROS, reactive oxygen species.

indicate that FA treatment may protect against neuronal death through the inhibition of miRNA-9 induction in the rat hippocampus following hypoxic-ischemic damage.[44,45]

It has been suggested that infections, inflammatory processes may be causative factors in emotional disorders, including anxiety and depression.[46,47] LPS injection resulted in significant impairment of memory function,[48] the present study was designed to examine the AD-like behavior and depressive-like response following intraperitoneal injections of LPS (200 μg/kg).

As shown in Figure 3H and F, the time spent in the plat form area and the number of crossing the plat form area of LPS group and 25 mg/kg FA group were significantly decreased compared with control group. It indicated that LPS-treated groups experienced high levels of memory deficit or depression. Moreover, AD or depression-like behavior

Table 16 Degree Scores of Key Hub Proteins in the FA-Related PPI Network Identified by STRING Database

Target	Degree Score
EGFR	49
ESR1	47
PTGS2	45
CTNNB1	44
STAT3	44

Table 17 Molecular Docking Results of FA with Key Target Proteins

Entry	Ligand	Protein Name	PDB ID	Binding Energy (kcal/mol)
1	Ferulic Acid	EGFR	5ug9	−6.7
2	Ferulic Acid	ESR1	7nfb	−7.4
3	Ferulic Acid	PTGS2	5f19	−7.6
4	Ferulic Acid	CTNNB1	7afw	−5.2
5	Ferulic Acid	STAT3	6njs	−5.8

Abbreviations: EGFR, Epidermal Growth Factor Receptor; ESR1, Estrogen Receptor 1; PTGS2, Prostaglandin-Endoperoxide Synthase 2; CTNNB1, Catenin Beta 1; STAT3, Signal Transducer and Activator of Transcription 3; PDB, Protein Data Bank.

induced by LPS treatment cannot be dissociated from length and speed to find the plat form in this experiment, especially the length to find the plat form. In this regard, the rats of the LPS groups showed depression and anxiety condition with regard to the swimming speed and length. Our data revealed that decreasing of the time spent in the plat form area and the number of crossing the plat form area of LPS treated rats could not only be interpreted in terms of AD, but also fear and anxiety. Anxiety-like behavior could be related to diminished exploration in the swimming pool. In the present experiment, the significant decreases induced by LPS including distance swum in the target quadrant, number of crossing the hidden platform area, mean swimming speed in the probe trial test and duration in the hidden platform area, reflect AD or depression-like behavior in LPS-treated rats (Figure 3E–H). LPS has been established as an effective initiator of nigrostriatal dopaminergic neuronal death and produces AD symptoms in experimental animals.[49,50] However, it is suggested that LPS exposure increased anxiety like behaviors and stress response in adult rats.[51] Interestingly, anxiety-like behavior is commonly seen as an symptom of AD.[52]

Microfluidic Technology as a Screening Platform for Lipid Nanocarrier Development

Our study validates microfluidic technology as an efficient screening platform for plant-derived compound formulations. While not directly measuring drug loading efficiency, this approach enables rapid evaluation of formulation feasibility through precise control of particle formation parameters.[31] The distinct physicochemical properties observed between FA-LNPs (80±3.2 nm, PDI=0.053) provided valuable early indicators for subsequent development prioritization.

Among various microfluidic methods, hydrodynamic focusing has emerged as the predominant approach since its initial application by Jahn et al.[53] Recent advances in microfluidic devices incorporating micromixers or electroformation systems have demonstrated particular promise.[54] These systems enable precise control over lipid-drug mixing through defined flow rates of organic and aqueous phases, resulting in uniform particle formation through rapid solvent dilution.

The microfluidic approach offers several advantages, including uniform particle size distribution, reproducibility, and process controllability through adjustable parameters (flow rates, ratios, and concentrations). Despite limitations in industrial

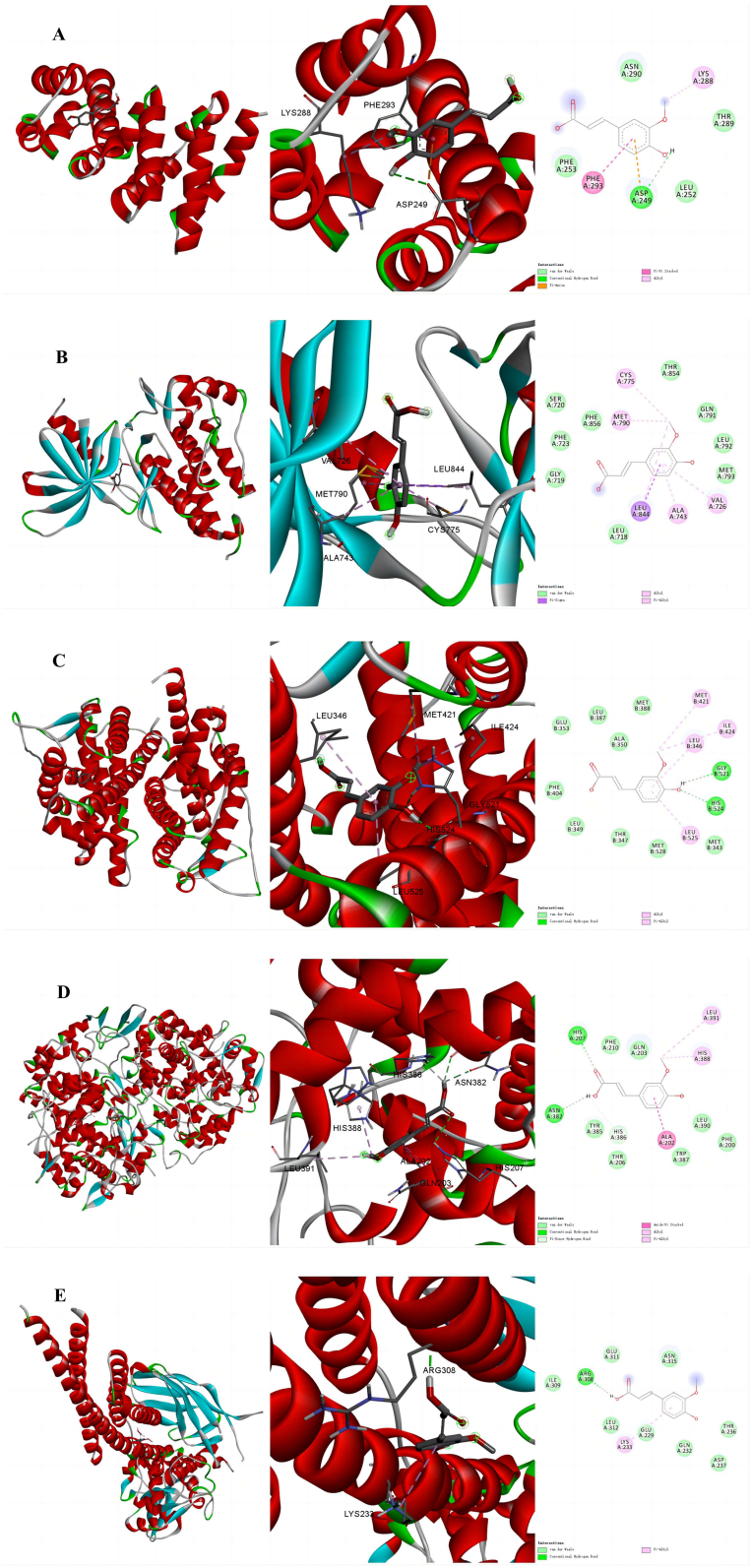

Figure 14 Molecular docking analysis revealing the binding modes of FA with key target proteins. (**A**–**E**) Two-dimensional (left panels) and three-dimensional (right panels) representations of FA interactions with (**A**) EGFR (PDB: 5ug9), (**B**) ESR1 (PDB: 7nfb), (**C**) PTGS2 (PDB: 5f19), (**D**) CTNNB1 (PDB: 7afw), and (**E**) STAT3 (PDB: 6njs). Hydrogen bonds are shown as green dashed lines, while hydrophobic and π-π stacking interactions are depicted in pink and Orange, respectively. Protein surface electrostatic potential is represented by different colors (red: negative, blue: positive, white: neutral). Binding energies were calculated ranging from −7.6 kcal/mol for PTGS2 to −5.2 kcal/mol for CTNNB1. **Abbreviations**: FA, ferulic acid; EGFR, epidermal growth factor receptor; ESR1, estrogen receptor 1; PTGS2, prostaglandin-endoperoxide synthase 2; CTNNB1, beta-catenin; STAT3, signal transducer and activator of transcription 3; PDB, Protein Data Bank.

scalability due to manufacturing complexity and throughput constraints, successful implementation in COVID-19 vaccine production by Pfizer/BioNTech and Moderna demonstrates its potential for large-scale applications.[55–57]

Multi-Technique Analytical Validation Strategy

Our comprehensive characterization approach integrated complementary analytical techniques to ensure robust formulation assessment. UPLC-MS/MS enabled precise molecular identification and quantification for drug loading and encapsulation efficiency evaluation, while DLS and TEM provided detailed insights into particle size distribution and morphology. This systematic approach aligns with established guidelines for nanomedicine characterization, particularly crucial for lipid nanoparticles where complex physicochemical properties necessitate thorough validation.[58]

Evolution and Optimization of Liposome Preparation Methods

Our systematic evaluation of three preparation methods revealed distinct advantages and limitations for each approach.[59] The conventional lipid film hydration method (Lipid Solubilization Method) demonstrated poor physical stability and suboptimal loading efficiency (3.10 mg/mL vs theoretical 5 mg/mL). These issues are consistent with recent studies highlighting the difficulties in encapsulating hydrophilic compounds using traditional liposome preparation methods.[60] The aqueous preparation method (Aqueous Preparation Method) also showed limitations, particularly in encapsulation efficiency, a common challenge in liposomal drug delivery systems.[61]

In contrast, the active loading method (Active Loading Method) demonstrated significant advantages, achieving efficient encapsulation and producing uniform liposomes. This aligns with recent advancements in active loading techniques for liposomal formulations.[62,63] The method's success in achieving high encapsulation efficiency (over 60%) is particularly noteworthy, as it addresses a key challenge in liposomal drug delivery.

The active loading method emerged as the optimal approach, achieving superior drug loading (≥4 mg/mL) and encapsulation efficiency (≥80%), highlighting the critical importance of method selection in liposome development.

Further experiments confirmed the reliability and scalability of the active loading method, producing liposomes with excellent parameters (FA concentration =4.98mg/mL, encapsulation efficiency (EE% =94.79%, particle size =131.4 nm, and PDI =0.126). These characteristics are crucial for effective drug delivery and are in line with current standards in nanomedicine.[64]

The physical stability of FA-LNPs was evaluated through zeta potential measurements under standardized conditions (25°C, water as dispersant). The nanoparticles exhibited a positive zeta potential of +5.97 mV with a quality factor of 1.701. Although this zeta potential value is relatively low compared to the conventional stability threshold (±30 mV), the formulation demonstrated remarkable stability in practice (more than 2 weeks).

The success of the active loading method in this study contributes to the growing body of evidence supporting its use in liposomal drug formulation. Recent studies have shown similar success with other challenging compounds, suggesting that this approach may have broad applicability in nanomedicine.[65]

Recent advances in liposome preparation techniques have demonstrated significant improvements in drug incorporation and stability.[66] Notably, the development of multifunctional envelope-type nano devices (MEND) showed promising results, with octaarginine-modified formulations exhibiting 1000-fold higher transfection efficiency compared to conventional DNA/PLL complexes.[67]

The active loading technique, particularly effective for hydrophilic drugs, can enhance entrapment efficiency from 30–50% to >90% through transmembrane gradients.[68,69] However, despite these advantages, industrial-scale implementation remains challenging due to manufacturing complexity.[70]

The ongoing evolution of liposome preparation methods reflects a critical balance between formulation optimization and manufacturing feasibility. Future developments should focus on streamlining preparation processes while maintaining product quality, ultimately enhancing therapeutic outcomes through improved drug delivery efficiency.[71]

However, while the active loading method shows promising results, further research is needed to fully understand its mechanisms and potential long-term stability issues. This aligns with current trends in nanomedicine research, which emphasize the importance of understanding the fundamental principles underlying nanoparticle formation and stability.[72]

Nanotoxicological Perspective

Our comparative analysis revealed distinct formulation outcomes driven by compound-specific physicochemical properties. FA-LNPs demonstrated robust characteristics with successful scale-up to 40 mL, consistent size distribution, and high encapsulation efficiency (≥80%), while enhancing pharmacokinetic parameters and reducing toxicity risks for natural compounds.[66]

Over the past two decades, nanodrug delivery systems have emerged as a focal point in pharmaceutical and materials science research, showing immense potential in improving drug targeting, bioavailability, and therapeutic efficacy, particularly in oncology and neurological disorders.[73]

However, significant gaps remain in understanding their in vivo pharmacokinetics and tissue distribution characteristics, limiting their clinical application.[74] Cheng et al highlighted that nanodrugs exhibit markedly different in vivo behaviors compared to traditional small molecule drugs, including complex metabolic processes and unique tissue distribution patterns.[75] Certain nanoparticles demonstrate prolonged retention in reticuloendothelial system organs, potentially leading to unexpected toxicity or altered therapeutic efficacy.[76]

The physicochemical properties of nanomaterials significantly influence their in vivo behavior, though specific mechanisms remain incompletely understood.[77] Blanco et al emphasized the importance of establishing quantitative relationships between nanomaterial characteristics and biological behavior for rational design of safe nanodrug delivery systems.[28]

The pioneering work of Oberdörster et al in nanotoxicology revealed that nanomaterials may exhibit distinct toxicological properties from their bulk counterparts, necessitating new evaluation methods. Their research highlighted specific concerns, such as nanoparticle penetration into the central nervous system via olfactory neurons, warranting particular attention to neurotoxicity.[78] Fadeel et al further demonstrated the crucial role of thorough material characterization in nanotoxicology, showing strong correlations between specific physicochemical properties and toxicity profiles.[79]

Recent advances in nanomedicine safety assessment, as discussed by Choi and Frangioni, emphasize comprehensive evaluation of both short-term and long-term toxicity, including acute, chronic, and potential carcinogenic effects.[80] Understanding nanoparticle biodistribution has become crucial for safety and efficacy assessment, driving the development of more precise in vivo tracking methods. Fadeel and Garcia-Bennett's research extensively explored how surface properties influence toxicity and biocompatibility, emphasizing the importance of understanding nanoparticle-cell interactions, cellular uptake mechanisms, and potential induction of oxidative stress and inflammatory responses.[81] This integrated understanding of physicochemical properties and their biological implications continues to shape the development of safer and more effective nanotherapeutics.

Acute Toxicity Studies of FA-LNPs

This comprehensive study evaluated the extended acute toxicity and pharmacokinetics of FA-LNPs (FA-LNPs) following intravenous administration, providing crucial evidence for their potential clinical application.

The cage-side observations revealed generally good overall condition in all groups except the positive control (Supplementary Table 01). The mortality of two female animals in the LPS group on the second day post-administration likely relates to LPS-induced acute inflammatory response, consistent with previous reports on LPS toxicity.[82] The hunched posture and piloerection observed in the LPS and LPS+ FA-LNPs groups are typical signs of discomfort associated with inflammatory reactions.[13]

Body weight and food/water intake changes were primarily concentrated in the positive control group. Male animals exhibited significant weight loss ($P \leq 0.05$ or 0.01) 2–6 days post-administration, with reduced food and water intake in the first 1~2 days (Supplementary Table 02 to Table 04). These changes, likely due to LPS-induced systemic inflammation, were reversible, with parameters returning to levels comparable to the blank control by the third day of recovery. This pattern aligns with previous studies on LPS-induced sickness behavior.[83]

Clinical pathology results indicated limited impact of FA-LNPs on most hematological and biochemical parameters (Supplementary Table 05 to Table 06). The observed decrease in reticulocyte count and percentage in male animals of the

vehicle control group may suggest a mild effect of liposomes on the hematopoietic system, a phenomenon reported in some liposomal formulations.[84] The alterations in PLT, PCT, UA, K levels, and MCH in male animals of the positive control group likely reflect LPS-induced systemic inflammation and potential renal effects, consistent with known LPS toxicity profiles.[85] Based on histopathological examination results (as shown in Figure 8A–F), we systematically evaluated the effects of various treatment groups on major organs in rats. The liver, kidney, and heart tissues of control groups (blank control and Con-LNPs) maintained normal histological architectures without significant pathological alterations (Figure 8A), indicating that the carrier nanoparticles themselves caused no tissue damage to these vital organs. The absence of demyelination (LFB staining, Figure 9) further supports the neurological safety profile of FA-LNPs, highlighting their potential as CNS-targeted delivery systems without neuropathological risks.

Pharmacokinetic Characteristics of FA-LNPs

The pharmacokinetic profile of FA-LNPs provides valuable insights into their in vivo behavior. At a dose of 46.5 mg/kg, male and female SD rats showed Cmax values of 420,000 ± 29,513 and 318,667 ± 86,639 ng/mL, and AUC0-t values of 80,414 ± 10,778 and 93,885 ± 13,429 h*ng/mL, respectively, with no significant gender differences (Supporting Table 14). This suggests similar absorption and distribution characteristics in both sexes, a favorable attribute for potential clinical applications.[86]

The mean residence time (MRT0-t) of 2.83 ± 0.792 hours, coupled with an elimination half-life (t1/2) of 12.8 ± 1.88 hours, indicates a multi-compartmental model in SD rats. The terminal elimination half-life (t1/2β) being significantly longer than the MRT suggests potential for prolonged drug action, a characteristic that could enhance therapeutic efficacy.[87]

The systemic clearance (CLz/F) of 0.535 ± 0.0851 L/h/kg indicates moderate drug clearance, while the apparent volume of distribution (Vz) of 9.73 ± 1.25 L/kg suggests primary distribution in plasma and extracellular fluid with limited transmembrane permeability (Supporting Table 15). This distribution profile may help reduce drug accumulation in non-target organs, potentially minimizing toxicity risks.[88]

This study demonstrates that FA-LNPs exhibit good safety profiles and acceptable pharmacokinetic characteristics at the given dose. The pharmacokinetic data reveal favorable in vivo behavior, potentially enhancing the therapeutic efficacy of FA.

Temporal Dynamics and Neuroprotective Trends

Our integrated findings establish ferulic acid-loaded lipid nanoparticles (FA-LNPs) as a biocompatible nanoplatform with context-dependent neuroprotective properties. Comprehensive histopathological evaluation demonstrated no significant abnormalities in major organs following FA-LNP administration alone,[89] while preserving cytoarchitecture across experimental groups. This structural preservation persisted even under LPS-induced inflammatory conditions,[29] demonstrating formulation stability comparable to advanced antioxidant carriers.[90,91]

The temporal dynamics of FA-LNP effects present intriguing observations. Our immunohistochemistry analyses revealed significant LPS-induced neuroinflammatory responses, with GFAP staining showing substantial astrocyte activation ($p < 0.01$) (Figure 10A and B) [92,93] and IBA-1 staining indicating significant microglial activation, see Figure 11A and B. While acute-phase glial activation showed limited response to intervention with FA-LNPs, Fluoro-Jade staining revealed that FA-LNP treatment did not effectively attenuate LPS-induced neurodegenerative changes, and even showed a subtle trend towards increased neurodegeneration, although this did not reach statistical significance. This unexpected observation suggests the need for careful optimization of treatment parameters and thorough safety evaluation of nanoparticle-based interventions in neurological conditions. See Figure 12A and B.

This temporal discordance may reflect nanoparticle biodistribution kinetics influenced by inflammatory BBB alterations,[94] selective modulation of specific inflammatory pathways,[91] or enhanced phagocytic clearance through controlled microglial activation.[95]

From a translational perspective, while our results indicate that FA-LNPs did not significantly alleviate LPS-induced neuroinflammation within the four-day experimental period, the preserved safety profile positions FA-LNPs as a clinically viable candidate. However, therapeutic optimization requires addressing temporal intervention windows,[96] formulation

engineering through surface modifications,[97] and potential synergistic combinations with immunomodulators.[98] These considerations are particularly important given the complex nature of neuroinflammatory responses.

Network Pharmacology and Molecular Docking Analysis Reveal Multiple Therapeutic Targets of Ferulic Acid

The network pharmacology analysis identified 176 potential targets of FA using SwissTargetPrediction and Super-PRED databases. The intersection of these targets with 47,043 disease-related targets obtained from GeneCards, OMIM, CTD, and DisGenet databases revealed 141 common targets (Figure 13A and B). This significant overlap suggests that FA may exert its therapeutic effects by modulating multiple disease-related pathways, consistent with the multi-target nature of many natural compounds.[99]

PPI network analysis using the STRING database revealed a highly interconnected network of 141 nodes and 794 edges, indicating substantial functional relationships among the identified targets. The average degree value of 11.3 suggests these targets may be involved in critical biological processes. Five key targets were identified based on their high degree values: EGFR, ESR1, PTGS2, CTNNB1, and STAT3 (Figure 13C). These targets may play crucial roles in mediating FA's therapeutic effects and warrant further investigation.[33]

GO enrichment analysis provided insights into the biological processes, cellular components, and molecular functions associated with FA's targets. The analysis revealed 504 GO terms, including 59 cellular components, 324 biological processes, and 121 molecular functions (Figure 13D). Notably, FA's targets were primarily localized in the plasma membrane, cytoplasm, and transcription factor complexes, suggesting diverse cellular effects. Key biological processes included regulation of single-carbon metabolic processes, response to exogenous stimuli, inflammatory response, and cellular response to beta-amyloid, indicating FA's potential in modulating fundamental disease-related pathways.[34]

KEGG pathway enrichment analysis identified 118 significantly enriched pathways ($p < 0.05$). The most significantly enriched pathways included nitrogen metabolism, AGE-RAGE signaling pathway in diabetic complications, metabolic pathways, and chemical carcinogenesis-reactive oxygen species (Figure 13E). These findings suggest that FA may exert its therapeutic effects through modulation of multiple interconnected pathways, consistent with the complex nature of the diseases studied.[35]

Molecular docking analysis provided further insights into the binding affinity of FA with the five key targets identified (Figure 14A–D). The binding energies ranged from −7.6 kcal/mol (PTGS2) to −5.2 kcal/mol (CTNNB1), indicating moderate to strong binding affinities. These results support the potential direct interactions between FA and these key targets, providing a molecular basis for FA's observed therapeutic effects.[36]

While network pharmacology and molecular docking provide valuable insights, these computational approaches have limitations. Further experimental validation, including in vitro and in vivo studies, is necessary to confirm the predicted interactions and their biological significance.

Conclusion

This comprehensive investigation provides compelling evidence for the therapeutic potential of FA-LNPs while highlighting critical considerations for their development and application. Through systematic formulation development, we successfully established FA-LNPs using an optimized active loading method, achieving superior encapsulation efficiency (≥80%) and uniform particle size (<200 nm, PDI=0.126). The implementation of microfluidic technology proved valuable as an efficient screening platform for early-stage formulation development, while our multi-technique analytical validation strategy integrating UPLC-MS, DLS, and TEM ensured robust characterization of the nanoformulation.

Toxicological and pharmacokinetic assessments revealed favorable safety profiles and drug behavior characteristics. FA-LNPs demonstrated acceptable acute toxicity with minimal systemic effects, while exhibiting advantageous pharmacokinetic parameters including extended elimination half-life ($t1/2 = 12.8 \pm 1.88$ hours), moderate systemic clearance ($CLz/F = 0.535 \pm 0.0851$ L/h/kg), and appropriate volume of distribution ($Vz = 9.73 \pm 1.25$ L/kg). Notably, the gender-independent pharmacokinetic behavior suggests consistent therapeutic effects across populations.

In the context of neuroprotection, FA-LNPs showed the ability to preserve tissue cytoarchitecture under inflammatory conditions, though with complex temporal dynamics in neuroinflammatory response. Network pharmacology analysis identified 141 potential therapeutic targets and revealed five key molecular targets (EGFR, ESR1, PTGS2, CTNNB1, STAT3), with significant pathway enrichment in inflammation, oxidative stress, and metabolic regulation, providing crucial mechanistic insights into FA's therapeutic actions.

While these findings establish FA-LNPs as a promising therapeutic platform, several aspects warrant further investigation, including optimization of temporal intervention windows and dosing regimens, exploration of surface modifications for enhanced targeting, and evaluation of potential synergistic combinations with other therapeutic agents. Additionally, long-term safety and efficacy studies will be essential for clinical translation. The integration of advanced formulation techniques with comprehensive pharmacological analyses provides a solid foundation for the future development of targeted nanomedicine approaches in treating complex disorders, potentially offering new therapeutic strategies for challenging medical conditions.

Acknowledgments

This study was approved by the Ethics Committee of Chengdu Qingbaijiang District People's Hospital (Approval number: 20220403010018).

This research was funded by the Sichuan Medical Association (Grant No. S22025).

Disclosure

The authors report no conflicts of interest.

References

1. Murakami A, Kadota M, Takahashi D, et al. Suppressive effects of novel ferulic acid derivatives on cellular responses induced by phorbol ester, and by combined lipopolysaccharide and interferon-gamma. *Cancer Lett*. 2000;157(1):77–85. doi:10.1016/S0304-3835(00)00478-X
2. Hosoda A, Ozaki Y, Kashiwada A, et al. Syntheses of ferulic acid derivatives and their suppressive effects on cyclooxygenase-2 promoter activity. *Bioorg Med Chem*. 2002;10(4):1189–1196. doi:10.1016/S0968-0896(01)00386-8
3. Ou L, Kong LY, Zhang XM, Niwa M. Oxidation of ferulic acid by momordica charantia peroxidase and related anti-inflammation activity changes. *Biol Pharm Bull*. 2003;26(11):1511–1516.
4. Srinivasan M, Sudheer AR, Menon VP. Ferulic acid: therapeutic potential through its antioxidant property. *J Clin Biochem Nutr*. 2007;40(2):92–100. doi:10.3164/jcbn.40.92
5. Yan JJ, Cho JY, Kim HS, et al. Protection against beta-amyloid peptide toxicity in vivo with long-term administration of ferulic acid. *Br J Pharmacol*. 2001;133(1):89–96. doi:10.1038/sj.bjp.0704047
6. Wyss-Coray T. Inflammation in Alzheimer disease: driving force, bystander or beneficial response? *Nature Med*. 2006;12(9):1005–1015. doi:10.1038/nm1484
7. Lin TY, Lu CW, Huang SK, Wang SJ. Ferulic acid suppresses glutamate release through inhibition of voltage-dependent calcium entry in rat cerebrocortical nerve terminals. *J Med Food*. 2013;16(2):112–119. doi:10.1089/jmf.2012.2387
8. Anselmi C, Centini M, Andreassi M, et al. Conformational analysis: a tool for the elucidation of the antioxidant properties of ferulic acid derivatives in membrane models. *J Pharm Biomed Anal*. 2004;35(5):1241–1249. doi:10.1016/j.jpba.2004.04.008
9. Michels B, Zwaka H, Bartels R, et al. Memory enhancement by ferulic acid ester across species. *Sci Adv*. 2018;4(10):eaat6994. doi:10.1126/sciadv.aat6994
10. Kudoh C, Hori T, Yasaki S, Ubagai R, Tabira T. Effects of ferulic acid and angelica archangelica extract (Feru-guard((R))) on mild cognitive impairment: a multicenter, randomized, double-blind, placebo-controlled prospective trial. *J Alzheimers Dis Rep*. 2020;4(1):393–398. doi:10.3233/ADR-200211
11. Ozato K, Tsujimura H, Tamura T. Toll-like receptor signaling and regulation of cytokine gene expression in the immune system. *BioTechniques*. 2002;33(sup4). doi:10.2144/Oct0208
12. Kobayashi K, Hernandez LD, Galan JE, Janeway CA Jr, Medzhitov R, Flavell RA. IRAK-M is a negative regulator of toll-like receptor signaling. *Cell*. 2002;110(2):191–202. doi:10.1016/S0092-8674(02)00827-9
13. Dantzer R. Cytokine-induced sickness behavior: mechanisms and implications. *Ann NY Acad Sci*. 2001;933(1):222–234. doi:10.1111/j.1749-6632.2001.tb05827.x
14. Hayley S, Wall P, Anisman H. Sensitization to the neuroendocrine, central monoamine and behavioural effects of murine tumor necrosis factor-alpha: peripheral and central mechanisms. *Eur J Neurosci*. 2002;15(6):1061–1076. doi:10.1046/j.1460-9568.2002.01936.x
15. Parnet P, Kelley KW, Bluthe RM, Dantzer R. Expression and regulation of interleukin-1 receptors in the brain. Role in cytokines-induced sickness behavior. *J Neuroimmunol*. 2002;125(1–2):5–14. doi:10.1016/S0165-5728(02)00022-X
16. Sgarbossa A, Giacomazza D, Di Carlo M. Ferulic acid: a hope for Alzheimer's disease therapy from plants. *Nutrients*. 2015;7(7):5764–5782. doi:10.3390/nu7075246
17. Mancuso C, Santangelo R. Ferulic acid: pharmacological and toxicological aspects. *Food Chem Toxicol*. 2014;65:185–195. doi:10.1016/j.fct.2013.12.024

18. El-Hammadi MM, Arias JL. An update on liposomes in drug delivery: a patent review (2014-2018). *Expert Opin Ther Pat*. 2019;29(11):891–907. doi:10.1080/13543776.2019.1679767
19. Wen MM, El-Salamouni NS, El-Refaie WM, et al. Nanotechnology-based drug delivery systems for Alzheimer's disease management: technical, industrial, and clinical challenges. *J Control Release*. 2017;245:95–107. doi:10.1016/j.jconrel.2016.11.025
20. Soares S, Sousa J, Pais A, Vitorino C. Nanomedicine: principles, properties, and regulatory issues. *Front Chem*. 2018;6:360. doi:10.3389/fchem.2018.00360
21. Tinkle S, McNeil SE, Muhlebach S, et al. Nanomedicines: addressing the scientific and regulatory gap. *Ann NY Acad Sci*. 2014;1313(1):35–56. doi:10.1111/nyas.12403
22. Bulbake U, Doppalapudi S, Kommineni N, Khan W. Liposomal formulations in clinical use: an updated review. *Pharmaceutics*. 2017;9(2):12. doi:10.3390/pharmaceutics9020012
23. Mitchell MJ, Billingsley MM, Haley RM, Wechsler ME, Peppas NA, Langer R. Engineering precision nanoparticles for drug delivery. *Nat Rev Drug Discov*. 2021;20(2):101–124. doi:10.1038/s41573-020-0090-8
24. Pelaz B, Alexiou C, Alvarez-Puebla RA, et al. Diverse applications of nanomedicine. *ACS Nano*. 2017;11(3):2313–2381. doi:10.1021/acsnano.6b06040
25. Naqvi S, Panghal A, Flora SJS. Nanotechnology: a promising approach for delivery of neuroprotective drugs. *Front Neurosci*. 2020;14:494. doi:10.3389/fnins.2020.00494
26. Patra JK, Das G, Fraceto LF, et al. Nano based drug delivery systems: recent developments and future prospects. *J Nanobiotechnology*. 2018;16(1):71. doi:10.1186/s12951-018-0392-8
27. Zhou Y, Peng Z, Seven ES, Leblanc RM. Crossing the blood-brain barrier with nanoparticles. *J Control Release*. 2018;270:290–303. doi:10.1016/j.jconrel.2017.12.015
28. Blanco E, Shen H, Ferrari M. Principles of nanoparticle design for overcoming biological barriers to drug delivery. *Nat Biotechnol*. 2015;33(9):941–951. doi:10.1038/nbt.3330
29. Qin L, Wu X, Block ML, et al. Systemic LPS causes chronic neuroinflammation and progressive neurodegeneration. *Glia*. 2007;55(5):453–462. doi:10.1002/glia.20467
30. Lazzara F, Conti F, Giuffrida E, et al. Integrating network pharmacology: the next-generation approach in ocular drug discovery. *Curr Opin Pharmacol*. 2024;74:102425. doi:10.1016/j.coph.2023.102425
31. Huang Y, Liu C, Feng Q, Sun J. Microfluidic synthesis of nanomaterials for biomedical applications. *Nanoscale Horiz*. 2023;8(12):1610–1627. doi:10.1039/d3nh00217a
32. Hopkins AL. Network pharmacology: the next paradigm in drug discovery. *Nat Chem Biol*. 2008;4(11):682–690. doi:10.1038/nchembio.118
33. Szklarczyk D, Kirsch R, Koutrouli M, et al. The STRING database in 2023: protein-protein association networks and functional enrichment analyses for any sequenced genome of interest. *Nucleic Acids Res*. 2023;51(D1):D638–D646. doi:10.1093/nar/gkac1000
34. Gene Ontology C. The gene ontology resource: enriching a gold mine. *Nucleic Acids Res*. 2021;49(D1):D325–D334. doi:10.1093/nar/gkaa1113
35. Kanehisa M, Furumichi M, Sato Y, Ishiguro-Watanabe M, Tanabe M. KEGG: integrating viruses and cellular organisms. *Nucleic Acids Res*. 2021;49(D1):D545–D551. doi:10.1093/nar/gkaa970
36. Chen G, Seukep AJ, Guo M. Recent advances in molecular docking for the research and discovery of potential marine drugs. *Mar Drugs*. 2020;18(11). doi:10.3390/md18110545
37. Leyane TS, Jere SW, Houreld NN. Oxidative stress in ageing and chronic degenerative pathologies: molecular mechanisms involved in counteracting oxidative stress and chronic inflammation. *Int J Mol Sci*. 2022;23(13). doi:10.3390/ijms23137273
38. Wang H, Sun X, Zhang N, et al. Ferulic acid attenuates diabetes-induced cognitive impairment in rats via regulation of PTP1B and insulin signaling pathway. *Physiol Behav*. 2017;182:93–100. doi:10.1016/j.physbeh.2017.10.001
39. Behl T, Makkar R, Sehgal A, et al. Current trends in neurodegeneration: cross talks between oxidative stress, cell death, and inflammation. *Int J Mol Sci*. 2021;22(14). doi:10.3390/ijms22147432
40. Brimson JM, Prasanth MI, Malar DS, et al. Plant polyphenols for aging health: implication from their autophagy modulating properties in age-associated diseases. *Pharmaceuticals*. 2021;14(10). doi:10.3390/ph14100982
41. Zhou S, Dong X. Neuroprotective properties of ferulic acid in preclinical models of Alzheimer's disease: a systematic literature review. *Curr Med Chem*. 2022. doi:10.2174/0929867329666220906110506
42. Sultana R. Ferulic acid ethyl ester as a potential therapy in neurodegenerative disorders. *Biochim Biophys Acta*. 2012;1822(5):748–752. doi:10.1016/j.bbadis.2011.10.015
43. Rehman SU, Ali T, Alam SI, et al. Ferulic acid rescues LPS-induced neurotoxicity via modulation of the TLR4 receptor in the mouse hippocampus. *Mol Neurobiol*. 2019;56(4):2774–2790. doi:10.1007/s12035-018-1280-9
44. Zhou Y, Yan F, Han X, et al. NB-3 expression in endothelial cells contributes to the maintenance of blood brain barrier integrity in a mouse high-altitude cerebral edema model. *Exp Neurol*. 2022;354:114116. doi:10.1016/j.expneurol.2022.114116
45. Yao K, Yang Q, Li Y, Lan T, Yu H, Yu Y. MicroRNA-9 mediated the protective effect of ferulic acid on hypoxic-ischemic brain damage in neonatal rats. *PLoS One*. 2020;15(5):e0228825. doi:10.1371/journal.pone.0228825
46. Swiergiel AH, Dunn AJ. Effects of interleukin-1beta and lipopolysaccharide on behavior of mice in the elevated plus-maze and open field tests. *Pharmacol Biochem Behav*. 2007;86(4):651–659. doi:10.1016/j.pbb.2007.02.010
47. Ekdahl CT, Claasen JH, Bonde S, Kokaia Z, Lindvall O. Inflammation is detrimental for neurogenesis in adult brain. *Proc Natl Acad Sci USA*. 2003;100(23):13632–13637. doi:10.1073/pnas.2234031100
48. Kim SE, Ko IG, Park CY, Shin MS, Kim CJ, Jee YS. Treadmill and wheel exercise alleviate lipopolysaccharide-induced short-term memory impairment by enhancing neuronal maturation in rats. *Mol Med Rep*. 2013;7(1):31–36. doi:10.3892/mmr.2012.1160
49. Kim WG, Mohney RP, Wilson B, Jeohn GH, Liu B, Hong JS. Regional difference in susceptibility to lipopolysaccharide-induced neurotoxicity in the rat brain: role of microglia. *J Neurosci*. 2000;20(16):6309–6316.
50. Gao HM, Liu B, Zhang W, Hong JS. Synergistic dopaminergic neurotoxicity of MPTP and inflammogen lipopolysaccharide: relevance to the etiology of Parkinson's disease. *FASEB J*. 2003;17(13):1957–1959. doi:10.1096/fj.03-0203fje
51. Lin YL, Lin SY, Wang S. Prenatal lipopolysaccharide exposure increases anxiety-like behaviors and enhances stress-induced corticosterone responses in adult rats. *Brain Behav Immun*. 2012;26(3):459–468. doi:10.1016/j.bbi.2011.12.003

52. Romano A, Pace L, Tempesta B, et al. Depressive-like behavior is paired to monoaminergic alteration in a murine model of Alzheimer's disease. *Int J Neuropsychopharmacol*. 2015;18(4). doi:10.1093/ijnp/pyu020
53. Jahn A, Vreeland WN, Gaitan M, Locascio LE. Controlled vesicle self-assembly in microfluidic channels with hydrodynamic focusing. *J Am Chem Soc*. 2004;126(9):2674–2675. doi:10.1021/ja0318030
54. Zhang G, Sun J. Lipid in chips: a brief review of liposomes formation by microfluidics. *Int J Nanomed*. 2021;16:7391–7416. doi:10.2147/IJN.S331639
55. Verbeke R, Lentacker I, De Smedt SC, Dewitte H. The dawn of mRNA vaccines: the COVID-19 case. *J Control Release*. 2021;333:511–520. doi:10.1016/j.jconrel.2021.03.043
56. Fang E, Liu X, Li M, et al. Advances in COVID-19 mRNA vaccine development. *Signal Transduct Target Ther*. 2022;7(1):94. doi:10.1038/s41392-022-00950-y
57. Hassett KJ, Benenato KE, Jacquinet E, et al. Optimization of lipid nanoparticles for intramuscular administration of mRNA vaccines. *Mol Ther Nucleic Acids*. 2019;15:1–11. doi:10.1016/j.omtn.2019.01.013
58. Fan Y, Marioli M, Zhang K. Analytical characterization of liposomes and other lipid nanoparticles for drug delivery. *J Pharm Biomed Anal*. 2021;192:113642. doi:10.1016/j.jpba.2020.113642
59. Ghasemiyeh P, Mohammadi-Samani S. Solid lipid nanoparticles and nanostructured lipid carriers as novel drug delivery systems: applications, advantages and disadvantages. *Res Pharm Sci*. 2018;13(4):288–303. doi:10.4103/1735-5362.235156
60. Gu Z, Da Silva CG, Van der Maaden K, Ossendorp F, Cruz LJ. Liposome-based drug delivery systems in cancer immunotherapy. *Pharmaceutics*. 2020;12(11). doi:10.3390/pharmaceutics12111054
61. Zylberberg C, Matosevic S. Pharmaceutical liposomal drug delivery: a review of new delivery systems and a look at the regulatory landscape. *Drug Deliv*. 2016;23(9):3319–3329. doi:10.1080/10717544.2016.1177136
62. Hashim PK, Punnoth Poonkuzhi N, Madappuram Cheruthu N, Saher Kuruniyan M. Drug delivery systems for natural medicines in cancer therapy. *Curr Top Med Chem*. 2024. doi:10.2174/0115680266315985240710063754
63. Chen J, Hu S, Sun M, et al. Recent advances and clinical translation of liposomal delivery systems in cancer therapy. *Eur J Pharm Sci*. 2024;193:106688. doi:10.1016/j.ejps.2023.106688
64. Yang B, Song BP, Shankar S, Guller A, Deng W. Recent advances in liposome formulations for breast cancer therapeutics. *Cell Mol Life Sci*. 2021;78(13):5225–5243. doi:10.1007/s00018-021-03850-6
65. Jacob S, Kather FS, Morsy MA, et al. Advances in nanocarrier systems for overcoming formulation challenges of curcumin: current insights. *Nanomaterials*. 2024;14(8). doi:10.3390/nano14080672
66. Ashfaq R, Rasul A, Asghar S, Kovacs A, Berko S, Budai-Szucs M. Lipid nanoparticles: an effective tool to improve the bioavailability of nutraceuticals. *Int J Mol Sci*. 2023;24(21). doi:10.3390/ijms242115764
67. Kogure K, Moriguchi R, Sasaki K, Ueno M, Futaki S, Harashima H. Development of a non-viral multifunctional envelope-type nano device by a novel lipid film hydration method. *J Control Release*. 2004;98(2):317–323. doi:10.1016/j.jconrel.2004.04.024
68. Pidgeon C, McNeely S, Schmidt T, Johnson JE. Multilayered vesicles prepared by reverse-phase evaporation: liposome structure and optimum solute entrapment. *Biochemistry*. 1987;26(1):17–29. doi:10.1021/bi00375a004
69. Chen G, Li D, Jin Y, et al. Deformable liposomes by reverse-phase evaporation method for an enhanced skin delivery of (+)-catechin. *Drug Dev Ind Pharm*. 2014;40(2):260–265. doi:10.3109/03639045.2012.756512
70. Szoka F Jr, Papahadjopoulos D. Procedure for preparation of liposomes with large internal aqueous space and high capture by reverse-phase evaporation. *Proc Natl Acad Sci U S A*. 1978;75(9):4194–4198. doi:10.1073/pnas.75.9.4194
71. Shah S, Dhawan V, Holm R, Nagarsenker MS, Perrie Y. Liposomes: advancements and innovation in the manufacturing process. *Adv Drug Deliv Rev*. 2020;154-155:102–122. doi:10.1016/j.addr.2020.07.002
72. Pei J, Palanisamy CP, Natarajan PM, et al. Curcumin-loaded polymeric nanomaterials as a novel therapeutic strategy for Alzheimer's disease: a comprehensive review. *Ageing Res Rev*. 2024;99:102393. doi:10.1016/j.arr.2024.102393
73. Shi J, Kantoff PW, Wooster R, Farokhzad OC. Cancer nanomedicine: progress, challenges and opportunities. *Nat Rev Cancer*. 2017;17(1):20–37. doi:10.1038/nrc.2016.108
74. Hare JI, Lammers T, Ashford MB, Puri S, Storm G, Barry ST. Challenges and strategies in anti-cancer nanomedicine development: an industry perspective. *Adv Drug Deliv Rev*. 2017;108:25–38. doi:10.1016/j.addr.2016.04.025
75. Cheng CJ, Tietjen GT, Saucier-Sawyer JK, Saltzman WM. A holistic approach to targeting disease with polymeric nanoparticles. *Nat Rev Drug Discov*. 2015;14(4):239–247. doi:10.1038/nrd4503
76. Bertrand N, Leroux JC. The journey of a drug-carrier in the body: an anatomo-physiological perspective. *J Control Release*. 2012;161(2):152–163. doi:10.1016/j.jconrel.2011.09.098
77. Nel AE, Madler L, Velegol D, et al. Understanding biophysicochemical interactions at the nano-bio interface. *Nat Mater*. 2009;8(7):543–557. doi:10.1038/nmat2442
78. Oberdorster G, Oberdorster E, Oberdorster J. Nanotoxicology: an emerging discipline evolving from studies of ultrafine particles. *Environ Health Perspect*. 2005;113(7):823–839. doi:10.1289/ehp.7339
79. Fadeel B, Fornara A, Toprak MS, Bhattacharya K. Keeping it real: the importance of material characterization in nanotoxicology. *Biochem Biophys Res Commun*. 2015;468(3):498–503. doi:10.1016/j.bbrc.2015.06.178
80. Choi HS, Frangioni JV. Nanoparticles for biomedical imaging: fundamentals of clinical translation. *Mol Imaging*. 2010;9(6):291–310.
81. Fadeel B, Garcia-Bennett AE. Better safe than sorry: understanding the toxicological properties of inorganic nanoparticles manufactured for biomedical applications. *Adv Drug Deliv Rev*. 2010;62(3):362–374. doi:10.1016/j.addr.2009.11.008
82. Remick DG, Ward PA. Evaluation of endotoxin models for the study of sepsis. *Shock*. 2005;24(1):7–11. doi:10.1097/01.shk.0000191384.34066.85
83. Nemzek JA, Hugunin KM, Opp MR. Modeling sepsis in the laboratory: merging sound science with animal well-being. *Comp Med*. 2008;58(2):120–128.
84. Szebeni J. Complement activation-related pseudoallergy: a stress reaction in blood triggered by nanomedicines and biologicals. *Mol Immunol*. 2014;61(2):163–173. doi:10.1016/j.molimm.2014.06.038
85. van Lier D, Geven C, Leijte GP, Pickkers P. Experimental human endotoxemia as a model of systemic inflammation. *Biochimie*. 2019;159:99–106. doi:10.1016/j.biochi.2018.06.014

86. Gandhi M, Aweeka F, Greenblatt RM, Blaschke TF. Sex differences in pharmacokinetics and pharmacodynamics. *Annu Rev Pharmacol Toxicol*. 2004;44:499–523. doi:10.1146/annurev.pharmtox.44.101802.121453
87. Xi XN, Liu N, Wang QQ, et al. Pharmacokinetics, tissue distribution and excretion of ACT001 in Sprague-Dawley rats and metabolism of ACT001. *J Chromatogr B Analyt Technol Biomed Life Sci*. 2019;1104:29–39. doi:10.1016/j.jchromb.2018.11.004
88. Choi YH, Yu AM. ABC transporters in multidrug resistance and pharmacokinetics, and strategies for drug development. *Curr Pharm Des*. 2014;20 (5):793–807. doi:10.2174/13816128005140214165212
89. Li J, Long X, Hu J, et al. Multiple pathways for natural product treatment of Parkinson's disease: a mini review. *Phytomedicine*. 2019;60:152954. doi:10.1016/j.phymed.2019.152954
90. Han EL, Tang S, Kim D, et al. Peptide-functionalized lipid nanoparticles for targeted systemic mRNA delivery to the brain. *Nano Lett*. 2025;25 (2):800–810. doi:10.1021/acs.nanolett.4c05186
91. de Lima GG, Zakaluk ICB, Artner MA, et al. Enhancing barrier and antioxidant properties of nanocellulose films for coatings and active packaging: a review. *ACS Appl Nano Mater*. 2025.
92. Norden DM, Godbout JP. Review: microglia of the aged brain: primed to be activated and resistant to regulation. *Neuropathol Appl Neurobiol*. 2013;39(1):19–34. doi:10.1111/j.1365-2990.2012.01306.x
93. Wang M, Pan W, Xu Y, Zhang J, Wan J, Jiang H. Microglia-mediated neuroinflammation: a potential target for the treatment of cardiovascular diseases. *J Inflamm Res*. 2022;15:3083–3094. doi:10.2147/JIR.S350109
94. Wohlfart S, Gelperina S, Kreuter J. Transport of drugs across the blood-brain barrier by nanoparticles. *J Control Release*. 2012;161(2):264–273. doi:10.1016/j.jconrel.2011.08.017
95. Cabral H, Li J, Miyata K, Kataoka K. Controlling the biodistribution and clearance of nanomedicines. *Nature Rev Bioengineer*. 2024;2(3):214–232. doi:10.1038/s44222-023-00138-1
96. Toader C, Dumitru AV, Eva L, Serban M, Covache-Busuioc RA, Ciurea AV. Nanoparticle strategies for treating CNS disorders: a comprehensive review of drug delivery and theranostic applications. *Int J Mol Sci*. 2024;25(24). doi:10.3390/ijms252413302
97. Agrawal M, Saraf S, Saraf S, et al. Recent strategies and advances in the fabrication of nano lipid carriers and their application towards brain targeting. *J Control Release*. 2020;321:372–415. doi:10.1016/j.jconrel.2020.02.020
98. Hopkins C, Javius-Jones K, Wang Y, Hong H, Hu Q, Hong S. Combinations of chemo-, immuno-, and gene therapies using nanocarriers as a multifunctional drug platform. *Expert Opin Drug Deliv*. 2022;19(10):1337–1349. doi:10.1080/17425247.2022.2112569
99. Kibble M, Saarinen N, Tang J, Wennerberg K, Makela S, Aittokallio T. Network pharmacology applications to map the unexplored target space and therapeutic potential of natural products. *Nat Prod Rep*. 2015;32(8):1249–1266. doi:10.1039/c5np00005j